2008

Biomimetic Self -Assembled Nanomatrix For Bone Tissue Regeneration

Joel M. Anderson
University of Alabama at Birmingham

BIOMIMETIC SELF-ASSEMBLED NANOMATRIX FOR BONE TISSUE REGENERATION

by

Joel M. Anderson

Ho-Wook Jun, Ph.D., CHAIR
Susan L. Bellis, Ph.D.
Renato P. Camata, Ph.D.
Thomas L. Clemens, Ph.D.
Timothy M. Wick, Ph.D.

A THESIS

Submitted to the graduate faculty of The University of Alabama at Birmingham, in partial fulfillment of the requirements for the degree of Master of Science

Sections of thesis prepared previously in preparation for submission to *Biomaterials*

Format adapted for thesis

BIRMINGHAM, ALABAMA

2008

BIOMIMETIC SELF-ASSEMBLED NANOMATRIX FOR BONE TISSUE REGENERATION

JOEL M. ANDERSON

BIOMEDICAL ENGINEERING

ABSTRACT

Bone is a dense, connective tissue with an extracellular matrix (ECM) comprised of biological and organic/inorganic biphasic matrices. For this study, novel peptide amphiphile (PA) nanomatrices were synthesized to mimic the native bone ECM and evaluated with human mesenchymal stem cells (hMSCs) isolated from bone marrow. The ability of this nanoscale, biomimetic scaffold composed of PAs that are inscribed with cellular adhesive ligands to direct hMSC osteogenic differentiation without supplements, along with other cellular behaviors, was investigated. Typical osteogenic supplements include dexamethasone, β-glycerol phosphate, and ascorbic acid. The synthesized PA sequences were evaluated as two-dimensional nanomatrix coatings without the inorganic component. In the 2-D nanomatrix environment, it was hypothesized that the PA nanomatrix could induce osteogenic differentiation of hMSCs without the presence of soluble factors based only on the incorporated cell adhesive ligands. Three different ligand peptide sequences (i.e. RGDS, DGEA, KRSR) that promote either integrin- or non-integrin-mediated cell binding were isolated and functionalized within the PA nanomatrices. hMSCs were seeded on the designed PA nanomatrices to assess the influence of each ligand signal on cellular behaviors. Initial attachment results demonstrated the adhesive ligands within the nanomatrices could be individually recognized and invoke different cellular responses. Long-term studies assessed osteogenic differentiation. Analysis of alkaline phosphate and osteopontin

secretion, markers for osteogenic differentiation, found the RGDS-containing nanomatrix to be the most promising. Evaluations of hMSC morphology and mineral deposition provided further support. Overall, the results clearly suggested that the PA nanomatrix directs osteogenic differentiation without the aid of supplements by mimicking the native ECM, providing an adaptable environment that allows for different adhesive ligands and types of cell-mediated binding to influence cellular behaviors. This is a promising discovery that allows for future experiments to further explore osteogenic differentiation driven by ligand signaling within the PA nanomatrix, along with eventually incorporating the inorganic components. Altogether, this research model establishes the beginnings of a new versatile approach to regenerate bone tissues, along with a variety of other tissues, by closely following the principles of natural tissue formation.

ACKNOWLEDGMENTS

Special thanks to the Biomedical Engineering department at the University of Alabama at Birmingham. The authors gratefully acknowledge Melissa Chimento and the High Resolution Imaging Facility for all TEM imaging. We also thank the Mass Spectrometry/Proteomics Shared Facility for analyzing the molecular weights of all samples. This work was supported by the 2007 Intramural Pilot Grant from the BioMatrix Engineering and Regenerative Medicine Center at UAB awarded to HWJ. Support is also acknowledged from the NIH T32 predoctoral training grant program for JMA.

TABLE OF CONTENTS

Page

LIST OF FIGURES

LIST OF ABBREVIATIONS

ECM	extracellular matrix
PA	peptide amphiphile
hMSC	human mesenchymal stem cell
BMP	bone morphogenic protein
HA	hydroxyapatite
TTCP	tetracalcium phosphate
TCP	tricalcium phosphate
PG	proteoglycan
MMP-2	matrix metalloproteinase-2
MSC	mesenchymal stem cell
ALP	alkaline phosphatase
OPN	osteopontin
TEM	transmission electron microscope
HBTu	*o*-benzotriazole-*N*,*N*,*N*′,*N*′-tetramethyluroniumhexafluorophosphate
DiEA	diisopropylethylamine
DMF	dimethylformamide
TFA	trifluoroacetic acid
DI	deionized
TIPS	triisopropylsilane

DCM	methylene chloride
MALDI-TOF	matrix-assisted laser desorption ionization time of flight
DMEM	Dulbecco's Modified Eagle's Medium
FBS	fetal bovine serum
PBS	phosphate buffered saline
PCNA	proliferating cell nuclear antigen

INTRODUCTION

The most promising paradigm for regenerative medicine is to engineer a nanostructured environment that mimics the complex hierarchical order and self-assembled formation of native tissue, as opposed to trying to adopt traditional materials to a biomedical need. This approach is emphasized by the ongoing research of biomimetic scaffolds that employ a bottom-up tissue engineering approach. To capture the self-assembling complexity required, bioactive scaffolds need to emulate the intrinsic properties of the extracellular matrix (ECM), which is an intricate meshwork of proteins and polysaccharides with great cellular influence (Daley, Peters, & Larsen, 2008). Cell-ECM interactions directly regulate cell behaviors, such as cell proliferation, growth, survival, polarity, morphology, migration, and differentiation (Daley et al., 2008; Kleinman, Philp, & Hoffman, 2003). Furthermore, different ECM molecules can selectively affect many types of signaling transduction pathways based on their inscribed ligand sequences, including differentiation pathways (Streuli, 1999). Thus, biomimetic scaffolds can be tailored to precise tissue regenerative needs by incorporating specific cellular adhesive ligands. In particular, a biomimetic, self-assembling nanomatrix for bone regeneration can be designed to take advantage of these naturally occurring signaling processes.

Currently, the bone regenerative treatment options are limited, thus an alternative tissue engineering approach is needed. In this regard, a biomimetic nanomatrix scaffold that mimics the bone hierarchical structure has been proposed. At the nanostructure level, the bone hierarchical order consists of three phases – organic, inorganic, and

biological (Gupta et al., 2005). For this project, the biomimetic nanomatrix scaffold designed and studied for bone tissue regeneration only focused on mimicking the organic and biological phases, leaving the inorganic phase for future work. This nanoscale scaffold consists of ECM-mimicking peptide amphiphiles (PAs) to represent the organic phase, which self-assemble into higher order structures to support human mesenchymal stem cells (hMSCs). This PA self-assembly formation process results in an elaborate nanofiber meshwork, creating a nanomatrix environment to present the different integrin- and non-integrin-mediated binding signals incorporated into the designed PAs. It is hypothesized that this biomimetic nanomatrix model can control the osteogenic differentiation and other cellular behaviors of hMSCs based only on the cell adhesive ligand sequences inscribed into the PA nanomatrices and without the aid of osteogenic supplements, which typically include dexamethasone, β-glycerol phosphate, ascorbic acid, and/or bone morphogenic protein (BMP). To further illustrate this hypothesis model, the overall scheme, including the amino acid sequences of the isolated cell adhesive ligands to be tested, is shown in Figure 1. (A more in-depth description of each cell adhesive ligand sequence is provided on pages 16-18.)

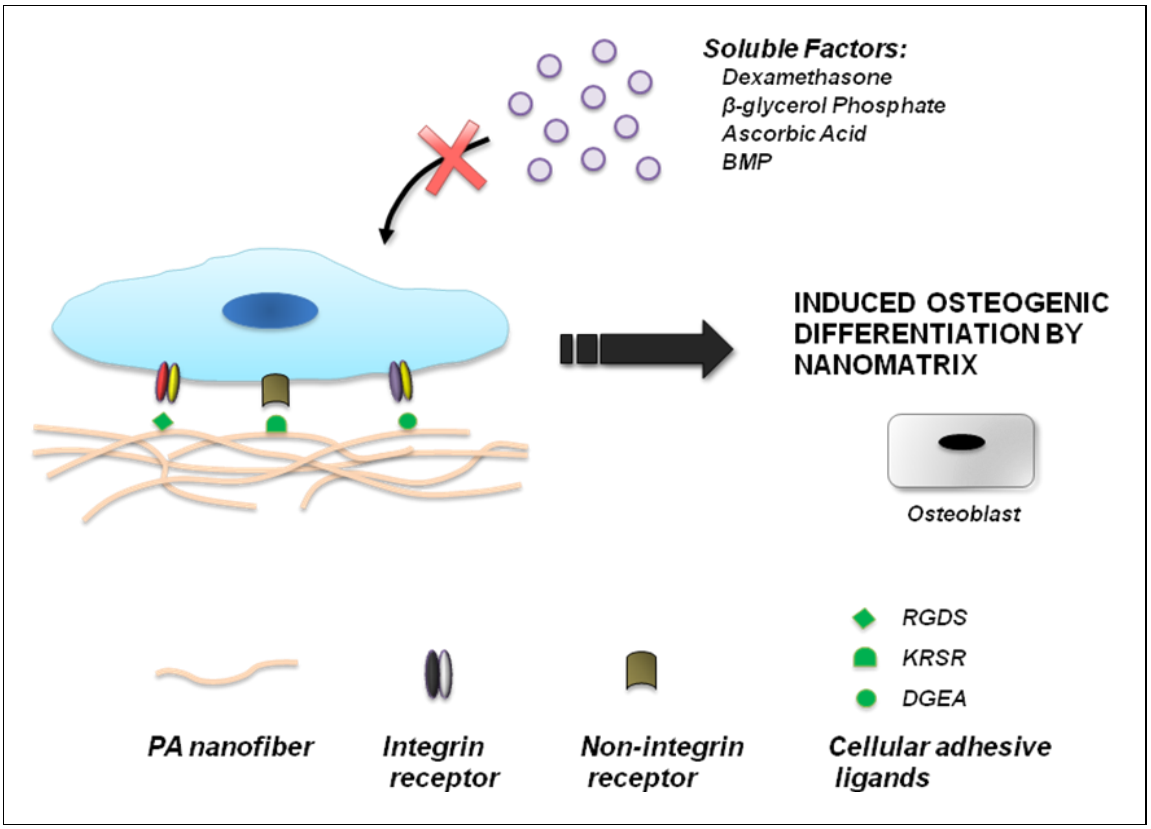

Figure 1. Schematic illustration of overall strategy for directing osteogenic differentiation based only on integrin- or non-integrin-mediated binding of specific cellular adhesive ligands incorporated into the PA nanofibers. No soluble factors were introduced to influence the hMSCs seeded on the PA nanomatrix coatings.

Overall, this study aims to investigate the osteogenic differentiating potential of hMSCs on the ECM-mimicking PA nanomatrices functionalized with different isolated ligand signals and without any aid from osteogenic stimulatory factors. A successful research model utilizing this biomimetic approach would have great potential for bone regeneration, demonstrating that osteogenic differentiation could be driven exclusively by cell-ligand interactions presented via the designed PA nanomatrix. Furthermore, it would provide insights into understanding essential bone tissue development, while at the same

time serving to develop a new strategy to regenerate a variety of tissues by closely mimicking the principles of natural tissue formation.

Bone Structure

Bone, itself, is a dense, connective tissue that is vital for movement, support, organ protection, red and white blood cell production, and mineral storage. The hierarchical structure of bone is complex, consisting of many different components at various scales, as shown in Figure 2. The structural organization is as follows: (1) macrostructure – cancellous and cortical bone; (2) microstructure – haversian systems, osteons, and single trabeculae; (3) sub-microstructure – lamellae; (4) nanostructure – fibrillar collagen and embedded mineral; and (5) sub-nanostructure – constitutive elements of crystalline minerals and collagen (Rho, Kuhn-Spearing, & Zioupos, 1998).

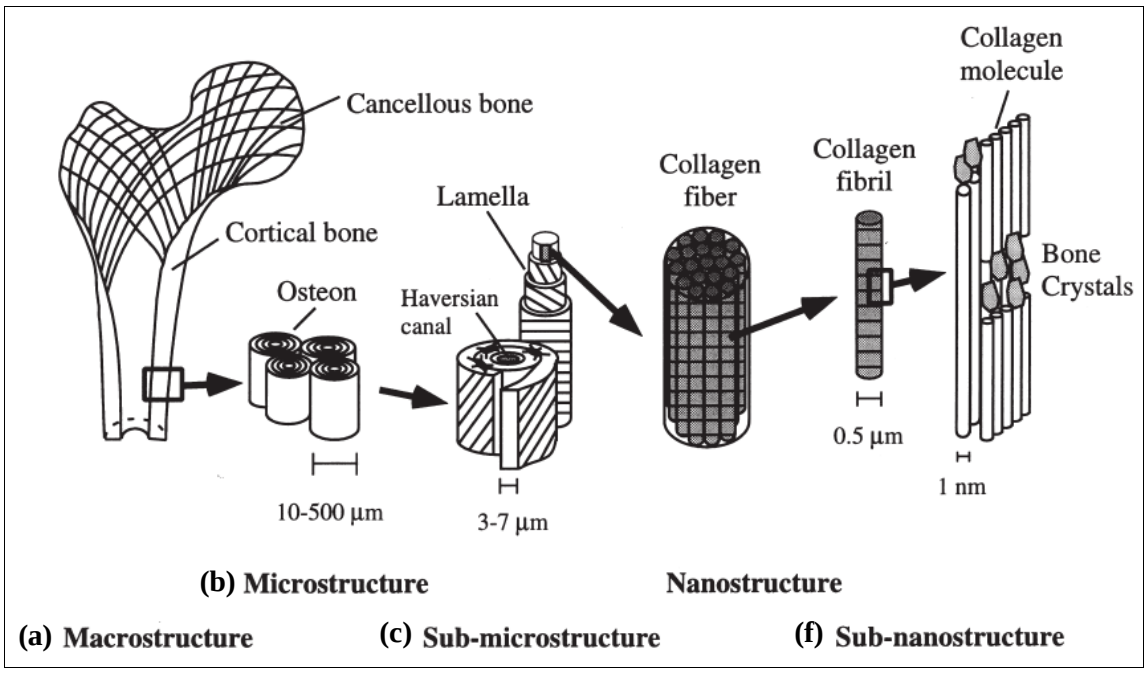

Figure 2. Hierarchical structural organization of bone: (a) cortical and cancellous bone; (b) osteons with Haversian systems; (c) lamellae; (d) collagen fiber assemblies of collagen fibrils; (e) bone mineral crystals, collagen molecules, and non-collagenous proteins.

From "Mechanical Properties and the Hierarchical Structure of Bone" by J.Y. Rho, L. Kun-Spearing, and P. Zioupos, 1998. *Medical Engineering & Physics*, *20*, p. 92. Copyright 1998 by Elsevier. Reprinted with permission.

The most basic building blocks of bone tissue are a composite of organic collagen molecules (300 nm long, 1.1 – 1.5 nm wide) interspersed with irregularly shaped inorganic bone crystals (3 – 5 nm thick), such as hydroxyapatite (HA) (Gupta et al., 2005). Therefore, the ideal strategy for bone tissue engineering is to mimic this nanoscopic natural self-assembly formation process.

Clinical Significance

Clinical needs for bone tissue regeneration encompass, but are not limited to, the regeneration of lost bone tissue and faster healing of bone fractures, especially non-union or delayed union fractures. Currently, the most common medical solution for bone treatment is bone grafting. According to the United States Census Bureau (2008), more than 1.6 million bone grafting procedures were performed in the United States in 2005 (*Statistical Abstract for the United States: Section 3 Health and Nutrition*, 2008). Additionally, it is estimated that of the 6 million fractures occurring annually in the United States, between 5% and 10% will result in non-union or delayed union (Nelson et al., 2003). Osteoporosis further contributes to the cause of bone loss. Osteoporosis is defined as a skeletal disorder characterized by compromised bone strength, predisposing to an increased risk of fracture (*Osteoporosis Prevention, Diagnosis, and Therapy Conference: Consensus Statement*, 2000). In the United States, 8 million women and 2 million men have osteoporosis (*America's Bone Health: The State of Osteoporosis and Low Bone Mass in our Nation*, 2002). Two million fractures each year in men and women over the age of 50 are attributed to osteoporosis, resulting in ~$17 billion in direct medical cost (Burge et al., 2007). While osteoporosis is the most wide-spanning of these medical problems, it is believed that the designed PA nanomatrix scaffold will have more immediate potential in the treatment of non-union or delayed union fractures. Therefore, bone tissue engineering has attracted great attention to solve all of these complicated and prevalent issues.

Previous Strategies for Bone Tissue Regeneration

The current treatment options for bone regeneration are autografts, allografts, and synthetic bone grafts. All have been extensively researched, and no definitive approach has emerged due to the variations that exist between patients, injury sites, and biological responses from the grafts. Autografts are the gold standard of bone grafting; however, this option is limited by low donor supply, donor site morbidity, and lengthening of the surgical procedure time due to two operating sites (Arrington, Smith, Chambers, Bucknell, & Davino, 1996; Schlegel et al., 2004; Wiltfang et al., 2004). Also, grafting is not a viable option for the elderly, children, or patients with malignant disease (Bridwell, O'Brien, Lenke, Baldus, & Blanke, 1994; Gau, Lonstein, Winter, Koop, & Denis, 1991; McCarthy, Peek, Morrissy, & Hough Jr, 1986). Allografts are the most frequently chosen bone substitute, and it is considered the second best treatment option behind autografts (Carter, 1999). Potential problems for this substitute are disease transmission, immunogenicity, increased cost, unavailability, and loss of biological and mechanical properties due to sterilization processing (Cowan, Soo, Ting, & Wu, 2005). In terms of demand, the number of bone grafting procedures in the United States has increased almost five-fold from 1990 to 2005, as shown in Figure 3 (*Statistical Abstract for the United States: Section 3 Health and Nutrition*, 2008).

[**As of end of year.** Based on reports of procurement programs and transplant centers in the United States, except as noted]

Procedure	Number of procedures						Number of centers		Number of people waiting, 2006	1-year patient survival rates, 2005 (percent)
	1990	1995	2000	2004	2005	2006	1990	2006		
Bone grafts (1,000). .	350	450	800	1,500	1,620	(NA)	30	64	(X)	(NA)

Source: U.S. Department of Health and Human Services, Health Resources and Services Administration, Office of Special Programs, Division of Transplantation, Rockville, MD; United Network for Organ Sharing (UNOS), Richmond, VA; University Renal Research and Education Association, Ann Arbor, MI; American Association of Tissue Banks, McLean, VA; and Eye Bank Association of America, Washington, DC; and unpublished data. See also <http://www.optn.org/>.

Figure 3. Organ transplants and grafts in the U.S. from 1990 to 2006. Adapted from the United States Census Bureau Statistical Abstract: Section 3 Health and Nutrition.

Thus, there is a huge need for alternative bone regeneration solutions. Consequently, synthetic bone substitutes have been researched in an effort to make up for the increased need. These implantable scaffolds can be characterized into three types by their biomaterial composition:

1) Inert – not stimulating bone formation
2) Osteoinductive – able to stimulate undifferentiated cells into osteoblasts
3) Osteoconductive – mature bone cells can attach, migrate, and proliferate

The current trends in bone regeneration research have shifted away from inert biomaterials, except for high load bearing applications (e.g. hip implants), and towards biocompatible osteoinductive and osteoconductive qualities. The ideal goal is to engineer a synthetic bone scaffold that exhibits the following properties: (1) biocompatible (i.e. non-toxic, non-immunogenic), (2) osteoconductive, (3) osteoinductive, (4) structurally stable, (5) bio-resorbable (i.e. degrades naturally at implant site), (6) bioresponsive (i.e.

scaffold degradation rate corresponds to correct healing rate), (7) easy to use for surgeon, and (8) cost effective (Cowan et al., 2005).

The types of synthetic scaffold biomaterials previously tested in bone healing models include: (1) polyesters, (2) collagen, (3) demineralized bone, (4) ceramics, (5) hydrogels, and (6) inert metals. Polyesters include polyglycolic acid, polylactic acid, and polyglycolic acid-co-lactic acid. These are the most widely investigated and commonly used synthetic, bioerodible polymers that degrade naturally *in vivo* via hydrolysis (Ratner, 1996). Potential applications include bone fixation devices, such as plates, screws, pins and nails, along with scaffolds for soft and hard tissue repair (Athanasiou, Niederauer, & Agrawal, 1996). Collagen is very prevalent in the bone ECM and contributes to mineral deposition, vascular in-growth, and growth factor binding, thus gaining interest as a bone substitute (Cornell, 1999). Demineralized bone is produced by decalcification of the cortical bone, along with further processing to reduce infection and immunogenic responses (Giannoudis, Dinopoulos, & Tsiridis, 2005). Ceramics are synthetic, inorganic materials, typically made from calcium phosphate, tricalcium phosphate (TCP), and/or hydroxyapatite. The more porous TCP degrades faster at the implant site, while HA is more permanent (McAndrew, Gorman, & Lange, 1988). Therefore, the two are often studied together at different mixture ratios to get the biomaterial properties desired. Hydrogels are water-swollen, cross-linked polymeric structures and have been made from gelatin and polyethylene glycol (Ratner, 1996). Inert metal bone substitutes can be manufactured from titanium or stainless steel. The benefits offered by these biomaterials include final control of structure, no immunogenicity, and high load bearing capacity (Cornell, 1999). No bone synthetic

substitute has emerged from these biomaterials as the most viable option. Thus, the most promising bone regeneration option will more than likely be a composite biomimetic scaffold, which incorporates many beneficial properties and contains biological components, such as osteogenic cells and osteoconductive growth factors. Current research is progressing in this direction, as combinations of surface modifications (e.g. HA), cell loading (e.g. stem cells), and growth factor incorporation (e.g. BMP) with different biomaterials are already being studied in hopes of regenerating natural bone tissue formations (Cowan et al., 2005).

Creating Biomimetic Self-Assembled Peptide Amphiphile Nanomatrix Scaffold

Our proposed bone regeneration solution is to develop a nanomatrix scaffold that recreates the natural building components of bone formation at the nanostructure level, thereby employing a bottom-up approach for tissue regeneration. This ideal bone biomimetic nano-composite scaffold will ultimately consist of ECM-mimicking peptide amphiphiles (PAs) as the organic component, biphasic phosphate (crystalline HA/resorbable TTCP) nanoparticles as the inorganic component, and human mesenchymal stem cells (hMSCs) isolated from bone marrow as the biological component, shown in Figure 4.

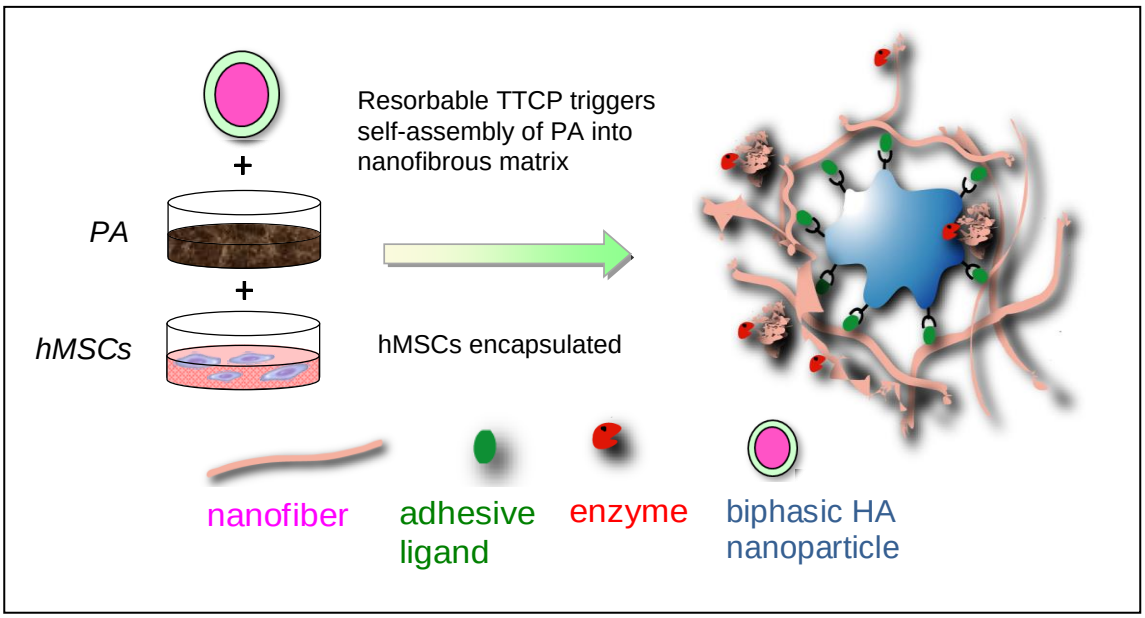

Figure 4. Schematic of bone ECM mimic organic/inorganic nanomatrix. It forms bone ECM mimic organization from self-assembly of hMSCs, organic-mimicking PA, and inorganic biphasic calcium phosphate nanoparticles.

It is believed that the dissolution of resorbable TTCP from inorganic biphasic calcium phosphates nanoparticles will trigger self-assembly of organic PAs into gel-like nanofibrous matrices, thereby encapsulating the hMSCs. Select cell adhesive ligand sequences and enzyme-mediated degradable sites in the PA, along with crystalline HA nanoparticles, will enable and coordinate biomineralization, growth, and differentiation of hMSCs into osteogenic cells, thus creating a biomimetic nanomatrix capable of controlling cellular functions for tissue regenerative medicine.

This biomimetic strategy presents an innovative but challenging approach to tissue regenerative medicine. The proposed composite scaffold offers the potential for inscribing cellular mimicking bioactive moieties, tunable mechanical properties of the organic/inorganic nanofibrous matrix, and a controllable self-assembly process. This construct would serve as a three-dimensional interface for cells, such as hMSCs,

harvested from natural tissue. The fabrication of the scaffold architecture at this nanoscale level is thought to be the best suited approach to facilitate cell-matrix interactions. The advantages of observing this level of detail are more natural cell adhesion and spreading within the three-dimensional framework (see Figure 5) (Stevens & George, 2005).

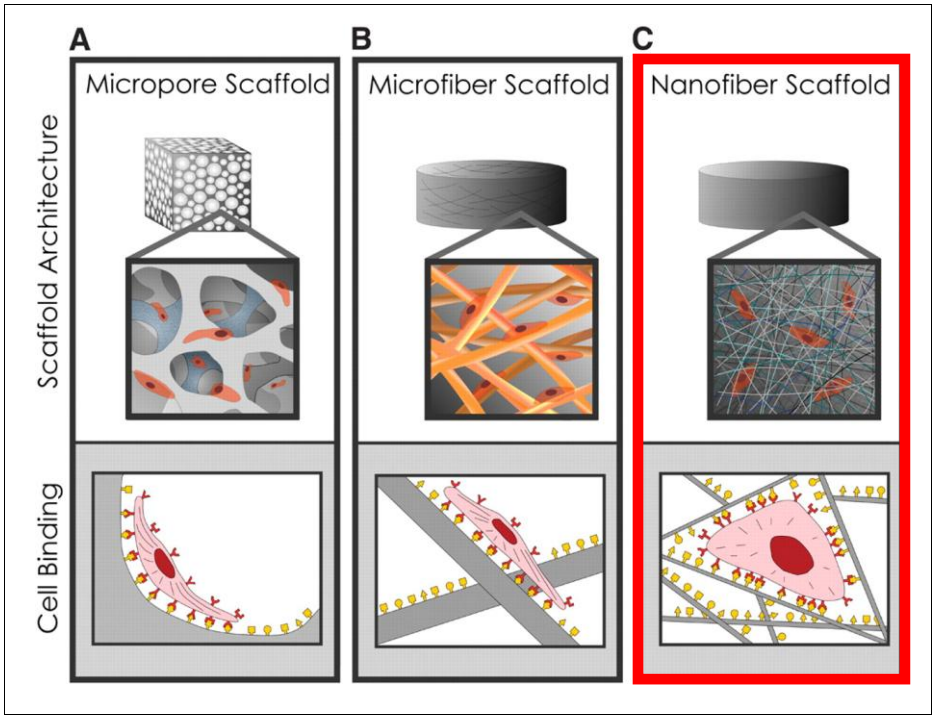

Figure 5. Scaffold architecture affects cell binding and spreading. (A and B) Cells binding to scaffolds with microscale architectures flatten and spread as if cultured on flat surfaces. (C) Scaffolds with nanoscale architectures have larger surface areas to adsorb proteins, presenting many more binding sites to cell membrane receptors.

From "Exploring and Engineering the Cell Surface Interface" by M.M. Stevens and J.H. George, 2005. *Science*, *310*, p. 1135. Copyright 2005 by AAAS. Reprinted with permission.

For the purpose of this thesis study, however, the goal was to first successfully synthesize the self-assembling PA nanomatrices and evaluate their potential to direct cellular behaviors in an *in vitro*, two-dimensional environment without inorganic minerals present. The 2-D studies, consisting of self-assembled PA coated layers, focused on the designed PAs and their ability to influence osteogenic differentiation and other cellular behaviors based only on the incorporated cell adhesive ligands and without the aid of supplements. This research was necessary to optimize future 2-D studies and gel encapsulation research, which will include the inorganic biphasic nanoparticles component.

Peptide Amphiphiles

Peptide amphiphiles (PAs) are a versatile material designed to mimic the organic nanoscale structure of bone tissue. In general, these amphiphilic molecules consist of a hydrophilic peptide segment, containing a varying amount of amino acids (6-15 residues), coupled via an amide bond to a hydrophobic alkyl chain that typically fluctuates in length from 10 to 22 carbon atoms (Beniash, Hartgerink, Storrie, Stendahl, & Stupp, 2005). Standard solid phase chemistry is used for synthesizing the peptide sequences. The general structural makeup of the PAs is a hydrophilic peptide segment that is ionic in nature and a single hydrophobic alkyl tail (J. D. Hartgerink, Beniash, & Stupp, 2001; Jun, Yuwono, Paramonov, & Hartgerink, 2005). However, PAs with multiple or branched alkyl tails have also been used in past research (Guler et al., 2006; Harrington et al., 2006; Lowik & Hest, 2004). Overall, PAs have been studied for an assortment of applications, ranging from functionalizing relatively inert surfaces with

bioactive signals (T. D. Sargeant et al., 2008; Sargeant, Rao, Koh, & Stupp, 2008), bone tissue regeneration (Hosseinkhani, Hosseinkhani, Khademhosseini, & Kobayashi, 2007; Hosseinkhani, Hosseinkhani, Tian, Kobayashi, & Tabata, 2007), drug delivery (Accardo, Tesauro, Mangiapia, Pedone, & Morelli, 2007; Rezler et al., 2007), blood vessel formation and angiogenesis (Hosseinkhani, Hosseinkhani, Khademhosseini, Kobayashi, & Tabata, 2006; Rajangam et al., 2006), and neural differentiation (Silva et al., 2004).

This material is advantageous because of its ability to self-assemble into sheets, spheres, rod-like fibers, disks, or channels, depending on the shape, charge, and environment (Israelachvili, Mitchell, & Ninham, 1977). For the purpose of this study, the PAs created self-assemble into cylindrical micelles when induced due to their conical shape in which the hydrophilic peptide segment is relatively bulkier than its narrow hydrophobic tail (J. D. Hartgerink, Beniash, & Stupp, 2002). Self-assembly creates an intricate nanomatrix environment. The nanomatrices are formed by a network of cylindrical nanofibers, ranging from 6 to 10 nm in diameter, depending on the length of the self-assembling molecules that form them (Beniash et al., 2005; Jun et al., 2005). They can achieve a length up to several microns (J. D. Hartgerink et al., 2001).

The amphiphilic nature of PAs is responsible for the nanofiber self-assembly process. The synthesized structures contain both polar and apolar elements, which tend to minimize unfavorable interactions in an aqueous environment by aggregating together, resulting in an arrangement with the hydrophilic domains being exposed to the outside and the hydrophobic sections remaining shielded within (Lowik & Hest, 2004). Primary methods for triggering nanofiber self-assembly are to alter the charge by adding divalent ions (i.e. Ca^{2+}) (Jun et al., 2005) or lowering the acidity (i.e. HCl) (J. D. Hartgerink et al.,

2001). These two methods create gel-like nanomatrices. In addition, PAs have also been observed to self-assemble when dried onto surfaces, allowing for two-dimensional studies (Harrington et al., 2006; Storrie et al., 2007). In this self-assembly method, the solvent is evaporated, leaving the PAs to aggregate together in a 2-D coating. For all induction methods, the self-assembled supramolecular structures are further stabilized by van der Waals and hydrophobic forces (see Figure 6) (Stendahl, Rao, Guler, & Stupp, 2006). Furthermore, because of the ionic nature of the molecule, self-assembly can be induced reversibly by changing the pH of the PA solution (J. D. Hartgerink et al., 2002). This reversibility allows for the material to respond to its environment by assembling, disassembling, or changing shape, especially as a self-assembled 3-D gel (J. D. Hartgerink, 2004).

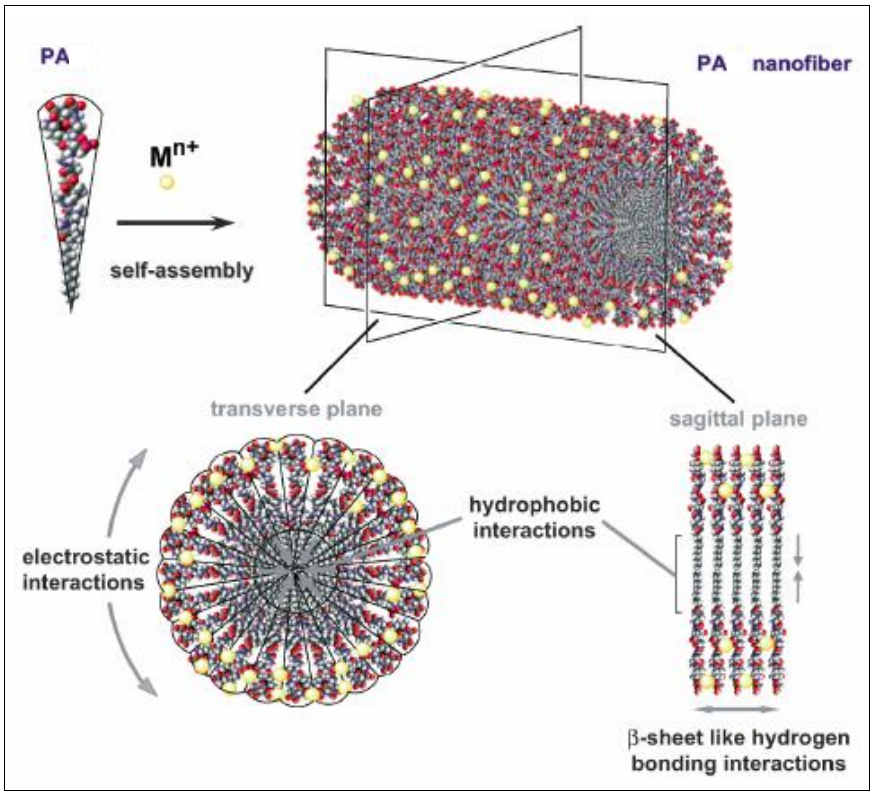

Figure 6. Scheme of peptide amphiphile nanofiber self-assembly via initial divalent ion induction, further stabilized by electrostatic and hydrophobic interactions.

From "Intermolecular Forces in the Self-Assembly of Peptide Amphiphile Nanofibers" by J.C. Stendahl, M.S. Rao, M.O Guler, and S.I. Stupp. Advanced Functional Materials, 6(4), p. 499. Copyright 2006 by Wiley-VCH Verlag GmbH & Co. KGaA. Reprinted with permission.

Cell Adhesive Ligand Sequences Incorporated into Peptide Amphiphiles

Recent trends in tissue engineering have shifted focus to creating bioactive materials that control cellular behaviors. Thus, three unique PA molecule structures have been developed and tested, each with a specific cellular adhesive ligand function according to the headgroup sequence. All PAs synthesized consisted of a cell adhesive ligand isolated from ECM proteins as the headgroup, enzyme degradable site specific for matrix metalloproteinase-2 (MMP-2), and hydrophobic alkyl tail (see Figure 7).

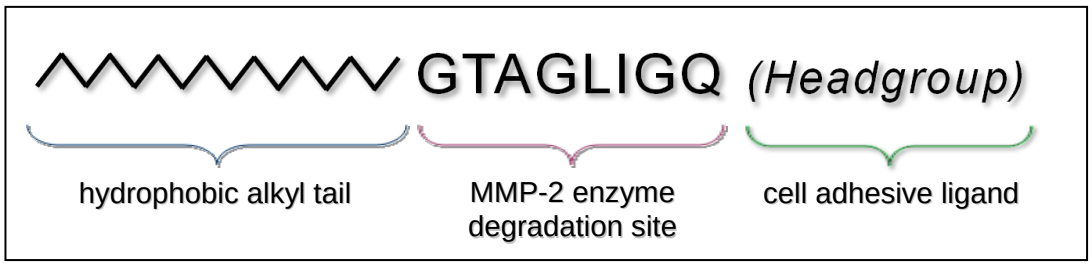

Figure 7. General schematic structure of peptide amphiphiles designed for project.

The following peptide cell adhesive ligand sequences were isolated and synthesized into the headgroups of the designed PAs: (1) Arg-Gly-Asp-Ser (RGDS), (2) Asp-Gly-Glu-Ala (DGEA), and (3) Lys-Arg-Ser-Arg (KRSR). RGDS functions as a general cell-adhesive sequence first developed by Pierschbacher and Rouslahti (1984). It exhibits predominant affinity for the integrins alpha5-beta1, alphaV-beta3, and alphaIIb-beta3 in cell adhesion (Hersel, Dahmen, & Kessler, 2003). The peptide sequence is the main recognition site for cell-surface integrins on fibronectin, a glycoprotein in the ECM. The RGDS moiety is located at the 10th type III module within the hairpin loop of fibronectin (Mardilovich, Craig, McCammon, Garg, & Kokkoli, 2006). This epitope can also be found in other ECM molecules, such as laminin, collagen type I, fibrinogen, vitronectin, von Willebrand factor, osteopontin, tenascin, and bone sialoprotein (Hersel et al., 2003). DGEA is a collagen type I adhesion motif. It plays a role in osteoblast adhesion via the alpha2-beta1 integrin, mediating extracellular signals into the cell (Harbers & Healy, 2005). Mizuno et al. found the DGEA interaction with the alpha2-beta1 integrin receptor important for signaling the osteoblastic differentiation of bone marrow cells (M. Mizuno, Fujisawa, & Kuboki, 2000; Morimichi Mizuno & Kuboki, 2001). The KRSR amino acid sequence binds to transmembrane proteoglycans in the ECM (Balasundaram & Webster, 2007). Proteoglycans (PG) constitute a large family of

complex molecules consisting of a core protein to which one or more linear carbohydrate chains are covalently attached. PGs play critical roles in connective tissue development and homeostasis (LeBaron & Athanasiou, 2000). By mimicking this ECM ligand signal, the KRSR motif has been found to increase osteoblast adhesion (Shin, Jo, & Mikos, 2003). For example, previous studies have shown that incorporating this moiety selectively increases osteoblast adhesion on nanograined titanium and micropatterned surfaces on borosilicate glass (Balasundaram & Webster, 2007; Hasenbein, Andersen, & Bizios, 2002). The final PA structural component is the Gly-Thr-Ala-Gly-Leu-Ile-Gly-Gln (GTAGLIGQ) peptide sequence that is an enzyme cleavable site specific for MMP-2 (Jun et al., 2005). MMP-2 is a highly conserved zinc-dependent enzyme secreted from the inside of the cell to the surface where it degrades most components of the basement membrane and ECM (Stefanidakis & Koivunen, 2006). Cleavage is expected between the glycine (Gly) and leucine (Leu) residues (Nagase & Fields, 1996). The incorporation of a MMP-2 specific sequence into the PA structure is projected to result in cell-mediated proteolytic degradation of the nanofiber network, enabling cell migration through the matrix and eventual remodeling of the matrix with natural ECM (Jun et al., 2005).

Hydroxyapatite and Tetracalcium Phosphate

For future nanomatrix scaffold designs outside the scope of this thesis project, calcium phosphates are to be incorporated to mimic the inorganic bone crystals in native tissue. Specifically, hydroxyapatite (HA) and tetracalcium phosphate (TTCP) will make up the biphasic inorganic component. These ceramic materials have good biocompatibility and bioactivity, as it can be directly bonded to bone (Guo, Xu, & Han,

2008). HA [$Ca_{10}(PO_4)_6(OH)_2$] is the most stable calcium phosphate under physiological conditions and considered a non-resorbable material (Guo et al., 2008; Kim, Camata, Vohra, & Lacefield, 2005). TTCP [$Ca_4(PO_4)_2O$] is created by the dehydroxylation of HA under melting conditions (Kim et al., 2005). TTCP degrades much more rapidly in the body than HA, and the ions released during TTCP resorption can aid in the bone formation at the interface between the biomedical implant and bone (Singh, de la Cinta Lorenzo-Martin, Gutiérrez-Mora, Routbort, & Case, 2006). Thus, HA and TTCP can be combined to create a tunable biphasic scaffold component. TTCP in a biphasic coating has been found to dissolve within 12 hours under simulated body fluid solution, while HA remains unaltered for at least one month (Kim et al., 2005). This allows for an adjustable degradation rate in which the balance between the in-growth rate of newly forming bone and scaffold resorption can be controlled as needed for different implantation sites (Guo et al., 2008). Furthermore, it has been demonstrated that divalent calcium ions can control the gelation and mechanical properties of the PA self-assembly process (Jun et al., 2005). So, the release of divalent calcium ions from TTCP during resorption offers the potential for a new PA nanofiber self-assembly induction method, which would allow for cell encapsulation when fully optimized.

Mesenchymal Stem Cells

The final component of the biomimetic nanomatrix is human mesenchymal stem cells (hMSCs) isolated from the bone marrow. The hMSCs provide the needed biological functionality, emulating the role naturally provided by osteogenic cells. The two main features of stem cells are self-renewal and the ability to propagate into different types of

mature cell lineages (Kimelman et al., 2007). hMSCs are adult stem cells, as opposed to embryonic or fetal stem cells. Thus, they are only able to repair or replace cells within certain tissue types in response to traumatic events or natural cell turnover (Jackson, Jones, Scotting, & Sottile, 2007). Stem cells remain present in adults throughout their lifetime; however, the amount decreases with age, typically reduced by half the original amount by the age of 80 (Fibbe & Noort, 2003).

Mesenchymal stem cells were first described by Friedenstein, Gorskaja, and Kulagina (1976) as clonal, adherent cells capable of differentiating into osteoblasts, adipocytes, and chondrocytes. Typically, they reside in the stromal region of the bone marrow, but have also been found in adipose tissue, umbilical cord blood, chorionic villi of the placenta, amniotic fluid, peripheral blood, fetal liver, lung, and exfoliated deciduous teeth (Bobis, Jarocha, & Majka, 2006). These unique, multipotent cells have the capacity to give rise to various types of mesenchymal tissues, such as muscle, connective tissue, and bones (Kimelman et al., 2007). Studies have shown that when properly stimulated, mesenchymal stem cells can differentiate into osteoblasts, chondrocytes, adipocytes, fibroblasts, myoblasts, cardiomyocytes, hepatocytes, tenocytes, and possibly even neurons (see Figure 8) (Bobis et al., 2006; Chen, Rousche, & Tuan, 2006).

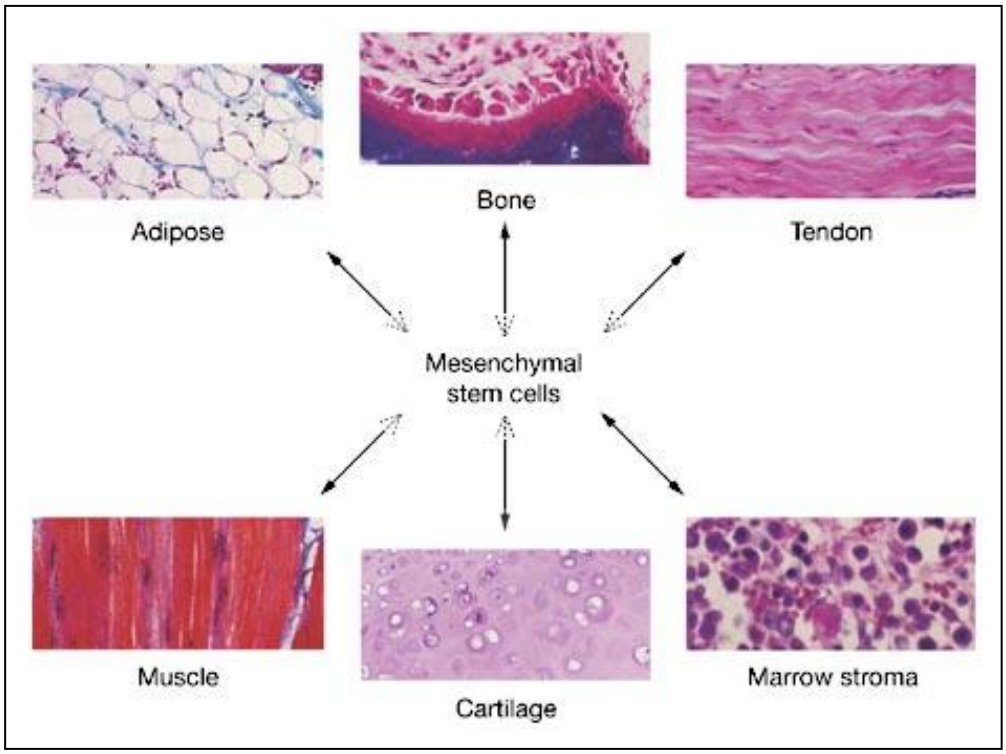

Figure 8. Multilineage differentiation potential of adult human mesenchymal stem cells.

From "Technology Insight: Adult Stem Cells in Cartilage Regeneration and Tissue Engineering" by F. Chen, K.T. Rousche, and R.S. Tuan. Nature Clinical Practice: Rheumatology, 2(7), p. 373. Copyright 2006 by Macmillan Publishers Ltd. Reprinted with permission.

hMSCs present an advantageous choice over osteoblasts for bone tissue regeneration using the designed biomimetic nanomatrix because of their versatility and potential to be applied to other tissues. They can be cultured and expanded *in vitro*, exhibiting spindle-like morphology when grown at low density (see Figure 9) and stacking into layers of flat cells with torn ends when confluency is reached. *In vitro* culturing allows for upscale production, as mesenchymal stem cells can be maintained for 20 – 30 population doublings and still retain their multipotent differentiation capability after *in vivo* implantation (Bobis et al., 2006). Furthermore, hMSCs offer the benefit of

low transplant risk for rejection and complications. Studies suggest that they have good immune system compatibility, exhibiting low MHC I and no MHC II expression (Jackson et al., 2007). Therefore, the vast proliferation potential, ability to differentiate into various cell types, and low immune response make mesenchymal stem cells an attractive tool for regenerative medicine.

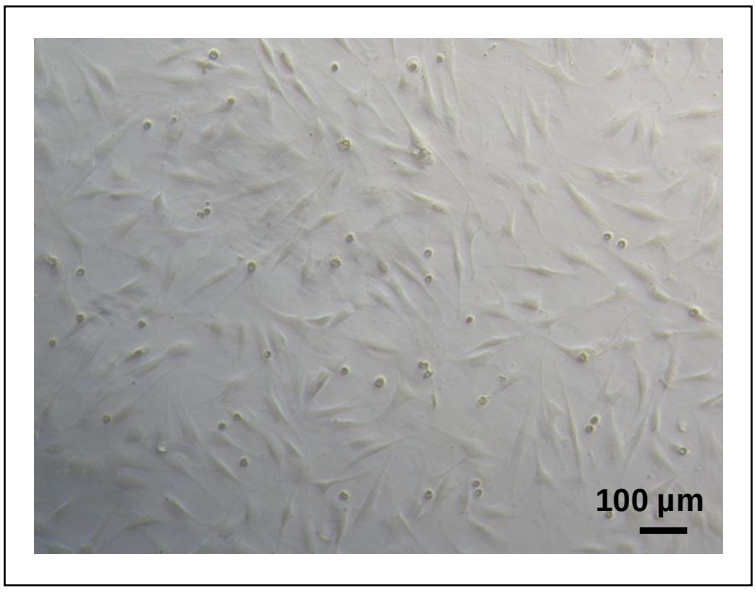

Figure 9. Bone marrow derived human mesenchymal stem cells cultured in Dulbecco's Modified Eagle's Medium supplemented with antibiotics.

Previous Studies to Differentiate Mesenchymal Stem Cells into Osteoblasts

The osteogenic differentiation of mesenchymal stem cells (MSCs) has been investigated on many different types of scaffolds, such as hydrogels, denatured type I collagen matrix, and self-assembling PAs. In most instances, soluble osteogenic factors were added to the media, such as dexamethasone, β-glycerol phosphate, ascorbic acid, and/or BMP. For example, hydrogels seeded with MSCs have been shown to promote

osteoblastic phenotypes in the present of supplements (Na et al., 2007). Yang et al. (2005) observed osteogenic differentiation on hydrogels modified with the RGD-peptide sequence, even finding an additive effect on differentiating potential as the RGD concentration increased. On denatured type I collagen, osteogenic differentiation of MSCs was also detected when the scaffold was supplemented with stimulatory factors (Mauney et al., 2006). For more studies detailing the osteogenic differentiation potential of MSCs in the presence of supplements, several comprehensive reviews exist in the literature (Gregory, Prockop, & Spees, 2005; Kimelman et al., 2007).

The purpose of this study was to control the differentiation and other cellular behaviors based only on the cell adhesive ligand sequences in the PA nanomatrix and without stimulatory factors. On self-assembled PA scaffolds, previous research has found rat MSCs to differentiate in the presence of osteogenic supplements, and the differentiating potential was observed to slightly increase in the added presence of the RGDS ligand (Hosseinkhani, Hosseinkhani, Tian, Kobayashi, & Tabata, 2006). However, hardly any studies have investigated the ability of cell adhesive ligands to solely guide osteogenic differentiation. In one such example, Shin *et al.* (2005) was able to induce the osteogenic differentiation of rat MSCs based only on cell adhesive ligand sequence, as the cells were seeded and differentiated on a RGD-modified hydrogel without dexamethasone and β-glycerol phosphate supplements. Overall, all of these studies taken together present conflicting results on the ability of cell adhesive ligands to direct osteogenic differentiation in the absence of media supplements or growth factors. This study aims to clear the confusion and fully investigate the osteogenic differentiating potential of several isolated ligand signals without any aid from traditional osteogenic

supplements. A successful research model utilizing this biomimetic approach would demonstrate that osteogenic differentiation could be driven exclusively by the PA nanomatrix and the cell-ligand interactions presented.

Osteoblast Differentiation Markers

The ability of the cellular adhesive ligands designed into the PAs to induce osteogenic differentiation will be evaluated by several markers. These osteogenic differentiation markers include alkaline phosphatase (ALP) activity, osteopontin (OPN) content, cell morphology, and mineral deposition. ALP is an enzyme that removes phosphate groups produced by osteoblasts. It is a widely used marker for osteoblasts, and an increase in activity is associated with early osteogenic differentiation (M. Mizuno et al., 2000). OPN is a major non-collagenous protein synthesized by differentiated osteoblasts and deposited into the mineralizing matrix (Morimichi Mizuno & Kuboki, 2001). It is employed as an osteogenic differentiation marker due to its association with cell attachment, proliferation, and mineralization of ECM in bone. Normal hMSC morphology is spindle-shaped; however, as osteogenic differentiation progresses, the cells change to a cuboidal appearance and begin to cluster together into multilayered colonies (Zhang et al., 2007). Finally, mineral deposition in the cellular environment serves as a late marker, indicating complete osteogenic differentiation (Shin et al., 2005). Mineralization can be analyzed qualitatively by histological staining, such as the von Kossa method. In von Kossa staining, silver nitrate binds to mineral deposits and produces identifiable brownish-black precipitates.

SPECIFIC AIMS

Scope of Study

Overall, the purpose of this research was to develop a biomimetic self-assembled nanomatrix for bone tissue regeneration by incorporating several cell adhesive ligands isolated from ECM proteins into peptide amphiphiles. The self-assembled nanomatrix was evaluated as two-dimensional coatings that present either integrin- or non-integrin-mediated binding based on the specific ligand signal. First, the conditions to induce self-assembly for 2-D coatings were identified and fine-tuned. This allowed the cellular behaviors of hMSCs to be evaluated in a 2-D environment. It was hypothesized that different responses would be observed based on the inscribed ligand signals, thus demonstrating that cellular behaviors, such as initial cell attachment and osteogenic differentiation, could be controlled by adhesive ligands. Of particular importance was directing osteogenic differentiation in the absence of supplemental aid based only on the cell-ligand interactions.

Specific Aim 1

Synthesize cell adhesive ligands into PAs and identify nanofiber self-assembly induction conditions for 2-D environment

All 2-D experiments used PA nanomatrix coatings that uniquely induced nanofiber self-assembly by solvent evaporation due to the resulting increased concentration and aggregation. Since several novel PAs with inscribed cell adhesive ligands were synthesized, evidence of self-assembly into nanofibers had to be confirmed for each coating. Furthermore, for the 2-D experiments to serve as a relevant comparison

to the future 3-D gel scaffold studies, it was imperative to prove that nanofiber self-assembly could be achieved. TEM imaging served as visual validation for all self-assembled PAs induced by solvent evaporation.

Specific Aim 2

Test ability of hMSCs to recognize and discern between the different cell adhesive ligands functionalized within 2-D PA coatings by evaluating initial cellular responses

Short-term experiments were conducted to ensure that the cells could recognize the cell adhesive ligands inscribed within the synthesized PAs. hMSCs were seeded onto the different PA nanomatrix coatings, and the elicited behavioral responses based on the different adhesive ligands were studied. It was believed that the isolated ligand signals within the each of the three coatings would trigger different cellular responses in attachment and proliferation. To substantiate this hypothesis, initial cell attachment and cellular proliferation experiments were performed, observing how the cells responded to the incorporated cell adhesive ligands. Furthermore, this specific aim served as a gateway to evaluating osteogenic differentiation over longer incubation periods.

Specific Aim 3

Induce osteogenic differentiation of hMSCs seeded on PA nanomatrix coatings based only on cell adhesive ligand signals and in the absence of osteogenic supplements

No osteogenic supplements, such as dexamethasone, β-glycerophosphate, or aspartic acid, were added to the culture media. This allowed osteogenic differentiation to be evaluated based only on the different cell adhesive ligands in the self-assembled PA

nanomatrix. hMSCs were seeded on the different PA nanomatrix coatings and incubated for three or more weeks. Alkaline phosphatase activity, osteopontin secretion, cell morphology, and mineral deposition via von Kossa staining were observed to determine the degree of osteogenic differentiation.

METHODS AND MATERIALS

Peptide Amphiphile Synthesis and Purification

The overall scheme for peptide amphiphile synthesis is depicted below in Figure 10. Three twelve-amino-acid peptides consisting of a MMP-2 sensitive sequence with cell-adhesive sequences RGDS (GTAGLIGQRGDS), DGEA (GTAGLIGQDGEA), or KRSR (GTAGLIGQKRSR) were synthesized by using standard Fmoc-chemistry on an Advanced Chemtech Apex 396 peptide synthesizer at a 0.30 mmol scale, similar to previously described PA syntheses (Jun et al., 2005; Paramonov, Jun, & Hartgerink, 2006). Alkylation was obtained by reacting the *N*-termini of the peptides with 2 equivalents of palmitic acid, 2 equivalents of *o*-benzotriazole-*N*,*N*,*N*′,*N*′-tetramethyluroniumhexafluorophosphate (HBTU), and 4 equivalents of diisopropylethylamine (DiEA) in dimethylformamide (DMF) for 12 hours at room temperature. After repeating the alkylation reaction once, cleavage and deprotection of the PAs were performed using a mixture of trifluoroacetic acid (TFA), deionized (DI) water, triisopropylsilane (TIPS), and anisole in the ratio of 40:1:1:1 for 3 hours at room temperature. The resulting solution for each was filtered, and the resin was rinsed with 20 mL of TFA. The collected samples were rotoevaporated and then precipitated in cold ether. The precipitates were collected and dried under vacuum using a lyophilizer. PAs were analyzed for impurities by matrix-assisted laser desorption ionization time of flight (MALDI-TOF) mass spectrometry.

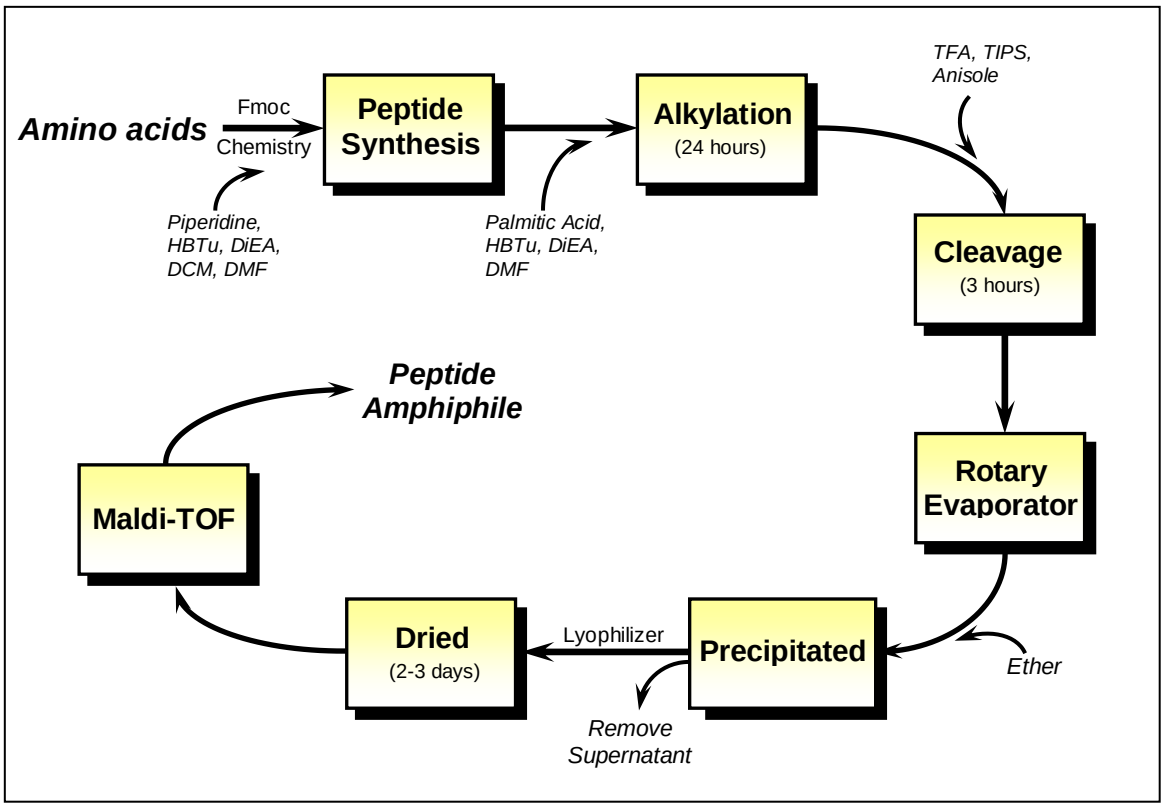

Figure 10: Schematic of process for peptide amphiphile synthesis.

Formation of Self-Assembled Peptide Amphiphile Nanofiber Coatings

A 0.1% wt. stock solution for each PA was prepared in DI water and adjusted to pH 7.4 by the addition of NaOH. From this PA stock solution, 200 µL per well were placed in 8-well silicone flexiPERM cell-culture chambers attached to glass cover slides. The chambers were placed in a chemical fume hood for 24 hours to evaporate the solvents and induce self-assembly. PA coatings were dried for two days in a 37°C incubator.

Transmission Electron Microscope Imaging

A 5 µL sample of each 0.1% wt. PA solution was applied to a carbon coated formvar cooper grid (400 mesh) and dried for 24 hours beforehand in a chemical fume hood to induce solvent evaporation self-assembly. The grids were negative stained with 10 µL of 20% phosphotungstic acid buffered to pH 7 for 30 seconds before wicking off excess. The samples were examined on a Tecnai T12 microscope by FEI operated at 60 kV accelerating voltage.

Cell Culture

hMSCs isolated from bone marrow were purchased from Lonza, Inc. (Walkersville, MD). hMSCs within passage number 3 – 6 were used for all experiments and grown with normal culture media: Dulbecco's Modified Eagle's Medium (DMEM; Mediatech, VA) prepared with 10% fetal bovine serum (FBS; HyClone, UT), 1% amphotericin B, 1% penicillin, and 1% streptomycin (Mediatech, VA). The PA coated 8-well flexiPERM cell-culture chambers were UV sterilized for 4 hours. The hMSCs were lifted using 0.25% trypsin/EDTA solution and re-suspended with normal culture media at a concentration of 300,000 cells/mL. A cell suspension of 100 µL (37,500 cells/cm^2) was seeded onto each PA coated culture chamber well. Cell cultures were maintained under standard culture conditions (37°C, 95% relative humidity, and 5% CO_2) with the media changes every 3-4 days. At given time points, the samples were removed and stored at -80°C. All collected samples were analyzed together for each biochemical assay.

Sample Preparation for Assays

Samples were prepared for measuring cellularity and ALP activity in the following manner. After 1 and 4 hours and on days 3, 7, 14, and 21, the cultured layers of hMSCs were washed with phosphate buffered saline (PBS) and incubated for 30 minutes at 37°C with 0.25% trypsin for detachment. The phenol red was removed from the trypsin to prevent any interference. The efficiency of removing the trypsinized cells was visually verified for each surface coating, as virtually all had been collected from each well. The collected cell samples were diluted with PBS at a 1:1 ratio and immediately stored at -80°C. On the day of each assay, the collected cell samples were lysed by a thaw/freeze cycle (30 minutes thawing at room temperature, 15 minutes of sonication, freezing at -80°C for 1 hour).

Analysis of Cellularity

The cell attachment for each time point was measured using a fluorometric PicoGreen DNA kit (Molecular Probes, OR) that quantifies the amount of double stranded DNA in cells. The fluorescent absorbance from the samples was measured using a microplate fluorescent reader (Synergy HT, BIO-TEK Instrument, VT) equipped with a 485/528 (EX/EM) filter set. A standard curve based on known concentrations of calf thymus DNA was used to determine the total amount of DNA. The cell number was calculated using 7.88×10^{-6} µg of DNA/cell, as determined by our lab for hMSCs.

Proliferating Cell Nuclear Antigen (PCNA) Staining

Self-assembled PA coatings were prepared on glass cover slides attached to 8-well silicone flexiPERM cell-culture chambers as described previously. hMSCs were seeded at 18,750 cells/cm^2 and incubated for 24 and 48 hours. At these two time points, the cells were fixed with 200 µL of formalin for 10 minutes and then rinsed with PBS. 200 µL of methanol were added for two minutes at room temperature to permeabilize the cells. After rinsing with PBS, the cells were incubated with 200 µL of 3% hydrogen peroxide for 5 minutes at room temperature, again rinsed with PBS, and soaked with Tris buffered saline for 5 minutes to remove any excess. The primary anti-PCNA antibody (Dako Corp., CA) and secondary anti-mouse IgG HRP antibody (Dako Corp., CA) solutions were both prepared at 1:100 dilutions. The fixed cells were labeled with 200 µL of the primary anti-PCNA antibody solution and incubated for 60 minutes at room temperature in a humidified chamber. After aspirating the antibody solution and rinsing with PBS, 200 µL of the secondary anti-mouse IgG HRP antibody were added, followed by another 60 minute incubation period at room temperature in a humidified chamber. Chromogenic substrate solution prepared from an AEC kit (Invitrogen, CA) was added to each well in 200 µL aliquots and incubated for 10 minutes. The samples were rinsed with PBS and counter stained with Mayer's hemotoxylin (Dako Corp., CA) for 5 minutes. Repeated rinsings with 200 µL of 37mM NH_4OH were performed until the solution turned blue, indicating removal of Mayer's hemotoxylin excess. The stained samples were then mounted and viewed under a phase contrast microscope. To quantify the percentage of PCNA positive cells, 5 random fields from each PCNA stained culture

chamber well were imaged, and the averaged ratio of proliferating cells compared to total cell number was calculated for each sample.

Alkaline Phosphatase Activity Assay

Aliquots of 60 µL cell lysates, 60 µL alkaline buffer, and 100 µL phosphatase substrate solutions were all added to a 96-well plate and incubated for 1 hour at 37°C. Standards in known concentrations ranging from 0 to 1000 µM were prepared using p-nitrophenol and added to designated wells in the same plate. After 1 hour of incubation, the kinase reaction was stopped by adding 100 µL of 0.3 M NaOH to each well. The absorbance of each well was measured using a microplate reader (EL x 800, BIO-TEK Instrument, VT) at 405 nm. The results were normalized to the total cell number at each time point measured by the PicoGreen DNA assay as previously described (see *Analysis of Cellularity*) and displayed as the amount of p-nitrophenol produced per cell after 1 hour incubation.

Osteopontin Secretion

The OPN secretion was analyzed using a human OPN TiterZyme enzyme-linked immunosorbent assay kit (Assay Designs, Inc., MI). The samples from the media secretion were collected and grouped together for the following time periods: days 4-7, 8-10, 11-14, 15-18, and 19-21. The results were expressed as OPN secretion concentration per day for each time interval. The standard solutions were prepared using a series dilution starting with the stock solution of human OPN (32 ng/mL). Performing the assay, 100 µL of standard solution or sample were added to the microtiter plate and

incubated at room temperature for 1 hour. The solutions in the wells were aspirated, followed by rinsing with 400 µL of washing buffer 4 times. Then, 100 µL of the antibody solution were added to each well before sealing the plate and incubating for 1 hour at room temperature. The antibody solution was aspirated, and the wells were rinsed 4 times using 400 µL of washing buffer. A volume of 100 µL of labeled conjugate solution was added to each well. The plate was sealed and incubated at room temperature for 30 minutes. All the well contents were emptied, and 100 µL of substrate solution were added to each well. The plate was again sealed, followed by another 30 minute incubation at room temperature. The reaction was stopped by adding 25 µL of the labeled stop solution to each well. The absorbance for all samples and standards was measured at 405 nm using the microplate reader (EL x 800, BIO-TEK Instrument, VT).

Mineral Deposition

This method histologically analyzed mineral deposition using the von Kossa method. Before fixing the cells for each sample, the cell morphology was recorded with phase contrast microscope imaging at each time, looking for characteristic signs of osteogenic differentiation. For von Kossa staining, the fixed cells were rinsed with 200 µL of PBS, stained with 400 µL of 5% silver nitrate, and exposed to UV light for 30 minutes. The reaction was stopped by adding 200 µL of 5% sodium thiosulfate to each sample for 5 minutes at room temperature. The samples were rinsed to remove any excess stain and imaged under the phase contrast microscope.

Statistical Analysis

All experiments were repeated at least twice with most being carried out three times or more. The graphical results are representative data sets performed in quadruplicate. All values are expressed as means ± standard deviation. SPSS 15.0 software (SPSS Inc., IL) was used to perform all statistical analysis. One-way analysis of variance (ANOVA) was used to assess significant differences. Tukey multiple comparisons test was also conducted to determine significant differences between pairs. For all statistical tests, $p<0.05$ was considered significant.

RESULTS

Two-Dimensional Nanofiber Self-Assembly

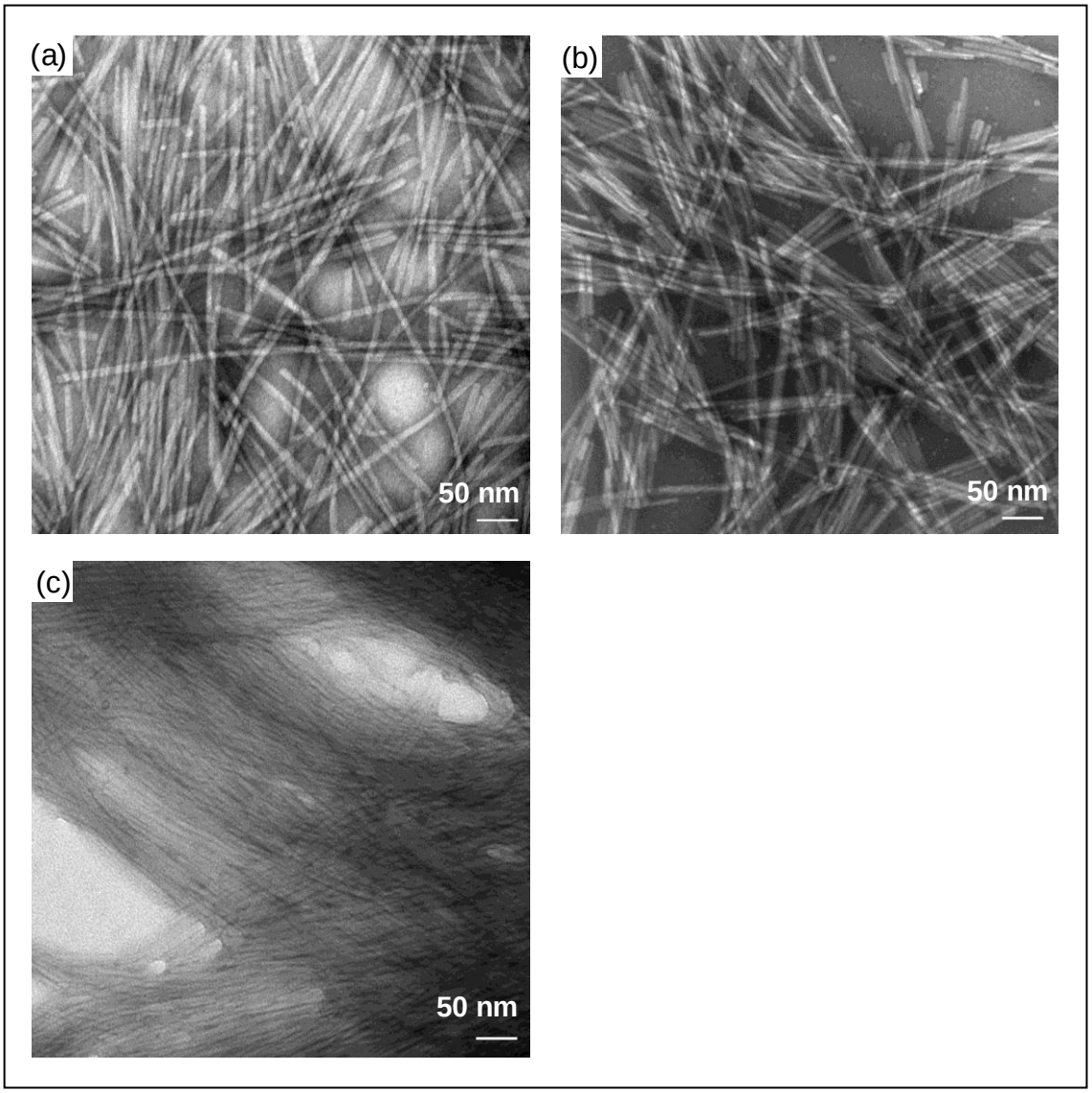

Figure 11. TEM images of solvent evaporation induced self-assembled nanofibers for the PA coatings of (A) PA-RGDS, (B) PA-DGEA, and (C) PA-KRSR.

Three PAs were designed with the following peptide sequences attached to a hydrophobic alkyl tail: (1) PA-RGDS [$CH_3(CH_2)_{14}CONH$ – GTAGLIGQ – RGDS], (2)

PA-DGEA [$CH_3(CH_2)_{14}CONH$ – GTAGLIGQ – DGEA], and (3) PA-KRSR [$CH_3(CH_2)_{14}CONH$ – GTAGLIGQ – KRSR]. The PAs were all successfully synthesized, as the molecular weights of PA-RGDS (MW=1369.97), PA-DGEA (MW=1326.92), and PA-KRSR (MW=1482.12) were all verified by MALDI-TOF mass spectrometry.

TEM imaging was used to characterize the self-assembled PA formations. Self-assembly was induced by evaporating the solvent from an aqueous PA solution (0.1% wt.) directly onto the TEM grid. The established self-assembly induction methods are adding divalent ions or lowering the pH (J. D. Hartgerink et al., 2001, 2002; Jun et al., 2005). As expected, TEM imaging in Figure 11 demonstrated successful cylindrical micelle nanofiber self-assembly for all novel PA sequences with this two-dimensional solvent evaporation coating method. Each of the PAs shown in Figure 11 is a representative image of the 2-D coatings chosen from at least 50 total images, thus indicating the high reproducibility of each PA surface condition. As evidenced, the nanofiber configuration is different for PA-KRSR compared to the other sequences. The nanofibers for PA-KRSR tended to be more aligned and bundled together. This is most likely due to the existing charge differences, as PA-KRSR is slightly more positive charged. However, as a whole, all of the nanofibers imaged were similar in size to past literature, exhibiting a uniform diameter of approximately 6–10 nm and length up to several microns (Jun et al., 2005). Also of interest is the solvent evaporation 2-D self-assembly induction method. Interestingly, other studies have used the solvent evaporation induction method, but none verified nanofiber self-assembly with TEM imaging or used the same PA sequences (Harrington et al., 2006; Storrie et al., 2007).

These observations prove that self-assembly of PAs can be achieved very simply by solvent evaporation, as the concentration of PAs reach the critical point needed for self-assembly.

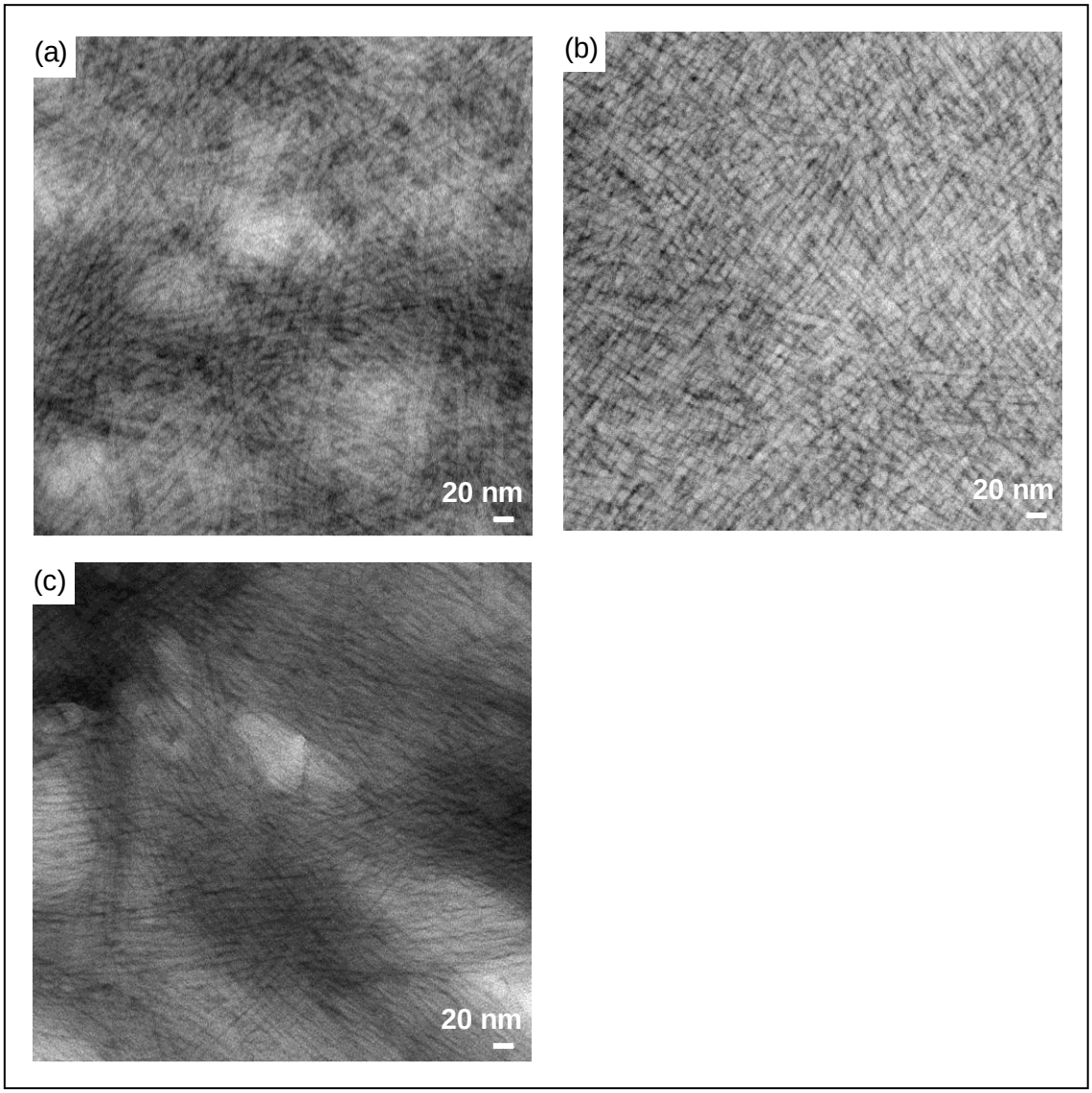

Figure 12. Multilayered TEM images of uniform 2-D PA coatings formed by solvent evaporation to create bulk self-assembled nanofiber networks of (A) PA-RGDS, (B) PA-DGEA, and (C) PA-KRSR.

Finally, to demonstrate the uniformity of each self-assembled PA surface condition at the microscale level, consistent multilayered nanofiber coatings were found for each PA. Specifically, the images in Figure 12 display the 2-D cell culturing environments presented by all three PA samples, as they consisted of numerous self-assembled nanofiber meshworks stacked on top of each other. As depicted, each PA was able to self-assemble into bulk nanofiber networks that entirely covered the surface area for all 2-D PA coatings. These self-assembled formations provided multilayered accessibility to the cell adhesive ligands functionalized within the outer hydrophilic domains. This finding demonstrates that the microscale self-assembling environment for all three PAs is uniform, thus relegating concerns of porosity, fiber orientation, and surface topography as non-issues.

Analysis of Cellularity

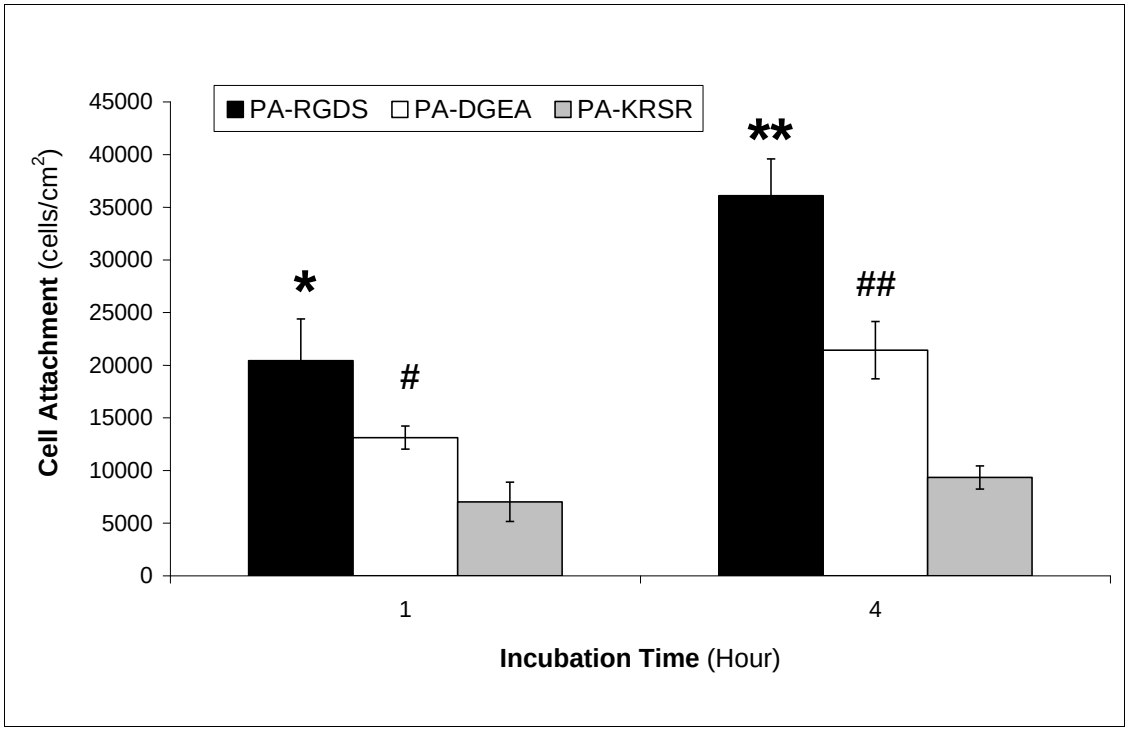

Figure 13. Initial attachment of hMSCs on PA coatings. *, **PA-RGDS promoted significantly greater cell attachment than PA-DGEA and PA-KRSR after 1 hour and 4 hours ($p<0.05$). #, ##PA-DGEA promoted significantly greater cell attachment than PA-KRSR after 1 and 4 hours ($p<0.05$). Error bar represents mean ± standard deviation.

First, the ability of the hMSCs to recognize the cell adhesive ligands within the PAs needed to be evaluated. This was accomplished with short-term studies characterizing the influence of the different cell-ligand interactions presented by the designed PAs. The initial cell attachment for 1 and 4 hours in Figure 12 was significantly higher on the PA-RGDS coating compared to the PA-DGEA and PA-KRSR coatings. Initial attachment increased ~50% between hour 1 (20400 ± 4000) and hour 4 (36100 ± 3500) for PA-RGDS. The PA-DGEA coating followed next with 13100 ± 1100 and 21400 ± 2700 cells/cm^2, respectively, exhibiting significantly greater attachment than PA-KRSR after 1 and 4 hours. Initial attachment to PA-KRSR essentially remained

constant for 1 and 4 hours with 7000 ± 1900 and 9300 ± 1100 cells/cm^2, respectively. Thus, the initial cell density is dependent on the inscribed signals present in the self-assembled PA coatings. This is similar to other studies where surfaces modified with RGDS-containing peptide sequences were found to exhibit greater cell attachment compared to DGEA or KRSR peptide sequences over short incubation periods (Harbers & Healy, 2005; Hasenbein et al., 2002).

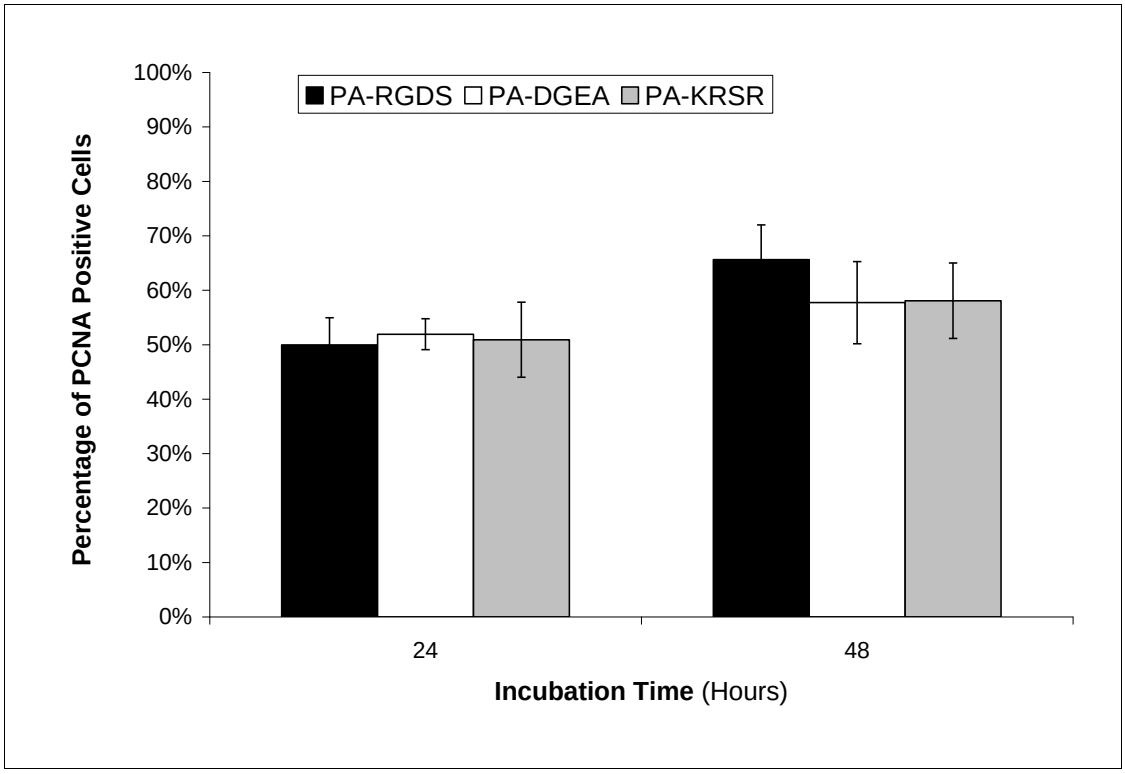

Figure 14. Proliferation of hMSCs seeded on the different PA nanomatrix coatings after 24 and 48 hours, quantitatively assessed by PCNA staining. Results are expressed as the percentage of PCNA positive cells. Error bar represents mean ± standard deviation.

Proliferating cell nuclear antigen (PCNA) is a 36 kd protein prevalent during the S-phase of the cell cycle, and it has a well established correlation to cell proliferation (Celis & Celis, 1985; Garcia, Coltrera, & Gown, 1989). Immunohistochemical labeling was used to evaluate hMSC proliferation on the different PA nanomatrices after 24 and 48 hours, as the percentage of positive PCNA stained cells compared to the total cell number was calculated for each sample (Figure 13). For all three PA nanomatrices, no significant differences in hMSC proliferation were observed, as each surface condition maintained a proliferation percentage between 50% - 70%, which is within the acceptable PCNA quantification range for normal human cells (Lynch et al., 1994). This finding

differs with the initial cell attachment results, which found cell density to be dependent on the ligand signals. Based on these results, any experimental differences observed after 48 hours, such as osteogenic differentiation potential for long-term studies, are not likely due to the proliferative ability of hMSCs and would more than likely be attributed to some other factor, such as the different cell-ligand interactions within the designed PA nanomatrices.

Alkaline Phosphatase Activity

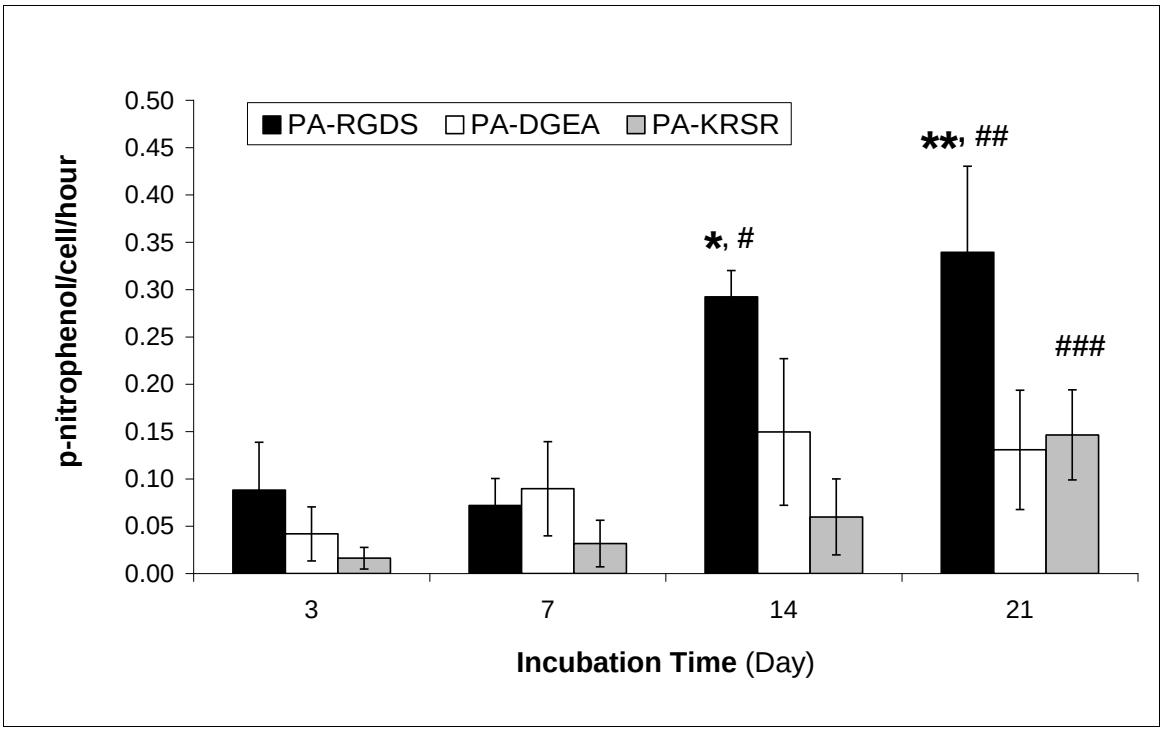

Figure 15. ALP activity of hMSCs on PA nanomatrices. ALP was measured using an end point enzyme assay and results are expressed as p-nitrophenol/cell/hour. *, **PA-RGDS exhibited significantly more ALP activity than PA-DGEA and PA-KRSR on days 14 and 21 ($p<0.05$). #, ##PA-RGDS expressed significantly more ALP activity on days 14 and 21 relative to days 3 and 7 ($p<0.05$). ###PA-KRSR showed significantly greater ALP activity on day 21 compared to days 3, 7, and 21 ($p<0.05$). Error bar represents mean ± standard deviation.

Alkaline phosphatase (ALP) is an enzyme that removes phosphate groups produced by osteoblasts. It is a widely used marker for osteoblasts, and an increase in activity is associated with early osteogenic differentiation (M. Mizuno et al., 2000). In Figure 14, PA-RGDS showed significantly greater ALP activity than PA-DGEA and PA-KRSR on days 14 (0.29 ± 0.03) and 21 (0.34 ± 0.09), respectively. Also, the ALP activity produced by PA-RGDS for days 14 and 21 increased significantly relative to days 3 (0.09 ± 0.05) and 7 (0.07 ± 0.03). The ALP activity of hMSCs on PA-DGEA

continually increased up to day 14 (0.15 ± 0.08) before plateauing. The PA-KRSR coating maintained a similar ALP activity range as PA-DGEA, slowly increasing in value up to day 21 (0.15 ± 0.05). The ALP activity for PA-KRSR was found to be significantly more on day 21 compared to the days 3 (0.02 ± 0.01), 7 (0.03 ± 0.02), and 14 (0.06 ± 0.04). However, the ALP activity values for PA-KRSR still remained much lower compared to PA-RGDS. Since ALP activity continually increased and never fully peaked for all PA coatings, later stage osteogenic differentiation may not be obtained after 21 days. Overall, the data suggests that the RGDS signaling peptide in the self-assembled PA coating promoted greater osteogenic differentiation of hMSCs compared to DGEA and KRSR coated surfaces.

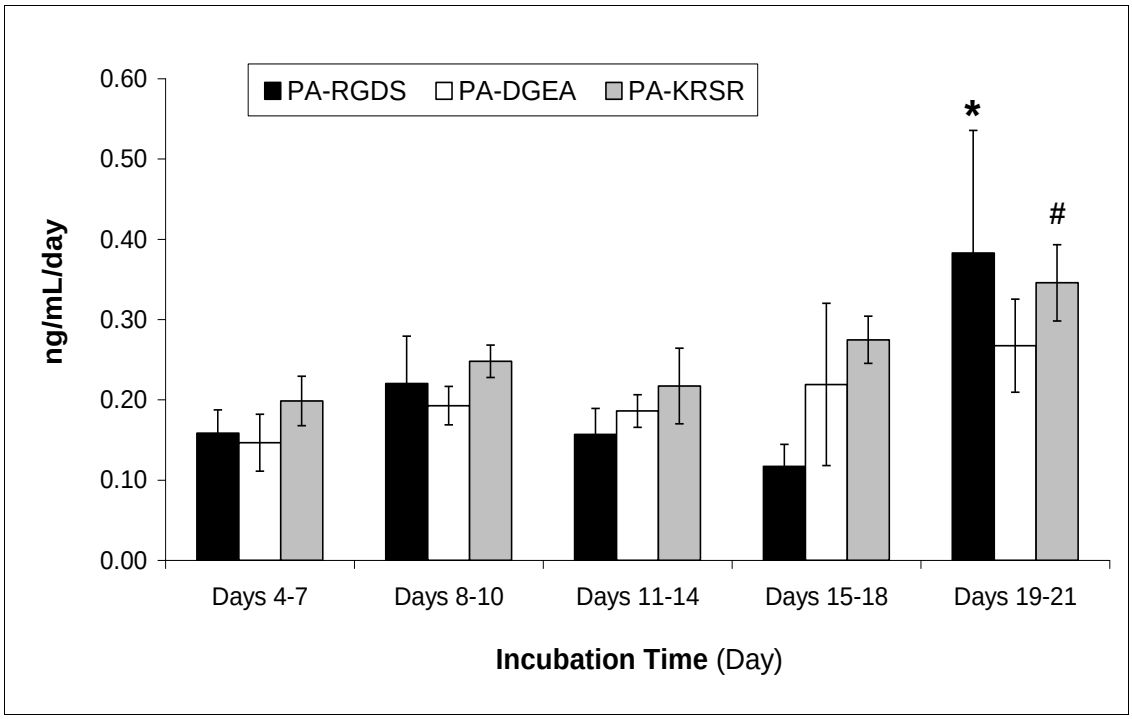

Figure 16. OPN secretion from hMSCs cultured on different PA nanomatrix coatings. Results are expressed as ng/mL/day. *PA-RGDS expressed significantly more OPN secretion on days 19-21 relative to days 4-7, 11-14, and 15-18 ($p<0.05$). #PA-KRSR showed significantly greater OPN secretion on days 19-21 compared to days 4-7, 8-10, and 11-14 ($p<0.05$). Error bars represent mean ± standard deviation.

Osteopontin (OPN) is a major non-collagenous protein synthesized by differentiated osteoblasts and deposited into the mineralizing matrix (M. Mizuno et al., 2000). It is employed as an osteogenic differentiation marker due to its association with cell attachment, proliferation, and mineralization of ECM in bone (Shin et al., 2005). To analyze OPN secretion from the hMSCs, culture media was collected every 3 – 4 days during routine changes. The accumulated amount of OPN collected between media changes was grouped together as days 4-7, 8-10, 11-14, 15-18, and 19-21. An ELISA assay was used to assess the OPN secretion based on each PA coating condition, and the

results are shown in Figure 15, expressed as the average concentration of OPN secreted per day. The OPN secretion produced from the hMSCs on PA-RGDS fluctuated before exhibiting a significant increase for days 19-21 (0.383 ± 0.153) relative to days 4-7 (0.16 ± 0.03), 11-14 (0.16 ± 0.03), and days 15-18 (0.12 ± 0.03). The PA-DGEA coating showed no significant increases over the entire incubation period, varying up and down while remaining relatively constant. The OPN secretion for PA-KRSR oscillated as well before displaying a significant increase for days 19-21 (0.35 ± 0.05) compared to days 4-7 (0.20 ± 0.03), 8-10 (0.25 ± 0.02), and 11-14 (0.27 ± 0.05). Overall, the general trend for OPN secretion on all PA nanomatrix surfaces was to rise and fall over the incubation period and reach the highest value by days 19-21. Furthermore, the results provide additional support to the ability of the RGDS cell adhesive ligand to influence osteogenic differentiation and give indications that the other ligand sequences may have some differentiating potential as well.

hMSC Morphology during Osteogenic Differentiation

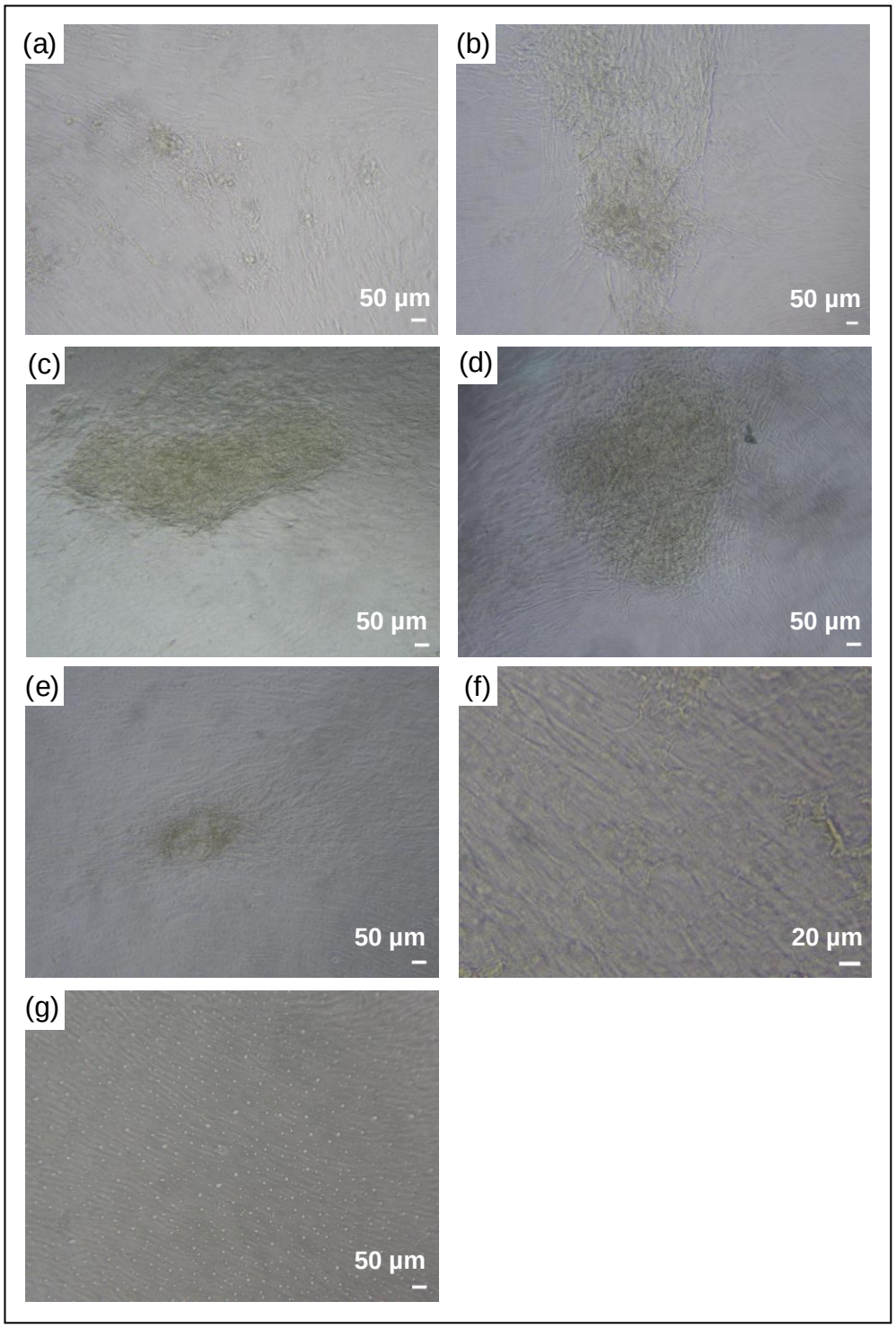

Figure 17. Phase contrast images of hMSCs to evaluate osteogenic morphology over a long-term incubation period on PA-RGDS after days 14 (a), 21 (b), 28 (c), and 35 (d). Further hMSC morphological images provided after 35 days for PA-DGEA (e), PA-KRSR (f), and glass (g).

Based on the osteogenic indicators of ALP activity and OPN secretion, later stage osteogenic differentiation of the hMSCs on the PA nanomatrix coatings did not appear to be fully reached after 21 days of incubation. Therefore, the cell morphology of the hMSCs was separately observed with phase contrast microscopy for up to 35 days. In general, there are three distinct phenotypes observed over the course of osteogenic development: (1) proliferating, (2) matrix maturation, and (3) mineralization (Kulterer et al., 2007). For hMSCs cultured on the three different PAs coatings plus glass as a reference, the most pronounced morphological changes were seen on the PA-RGDS coating, shown in Figure 16(a-d). After the initial proliferating phase, the hMSCs cultured on PA-RGDS started to morphologically change from spindle-shaped to cuboidal or polygonal by day 14, becoming increasingly more apparent by day 21. By days 28 and 35, the cuboidal cells began to form multilayered nodular colonies on PA-RGDS in an intermittent, island-like fashion. Conversely, the PA-DGEA coating (Figure 16e) was the only other surface condition to show signs of cell morphology change and colony clusters after 35 days. There were no such osteogenic appearances seen on the PA-KRSR culture samples (Figure 16f). Likewise, the hMSCs cultured on the control glass surface (Figure 16g) maintained their undifferentiated, spindle-shape morphology. Thus, the inscribed RGDS ligand signals appear to have the most impact on hMSC morphology when cultured without osteogenic supplements. This observed morphological shift and colony formation on the PA-RGDS nanomatrix indicates increased ECM production and subsequent mineral deposition, characteristic signs of osteogenic differentiation (Hayashi, Katsube, Hirose, Ohgushi, & Ito, 2008; Kulterer et al., 2007; Woll, Heaney, & Bronson, 2006; Zhang et al., 2007).

Mineral Deposition

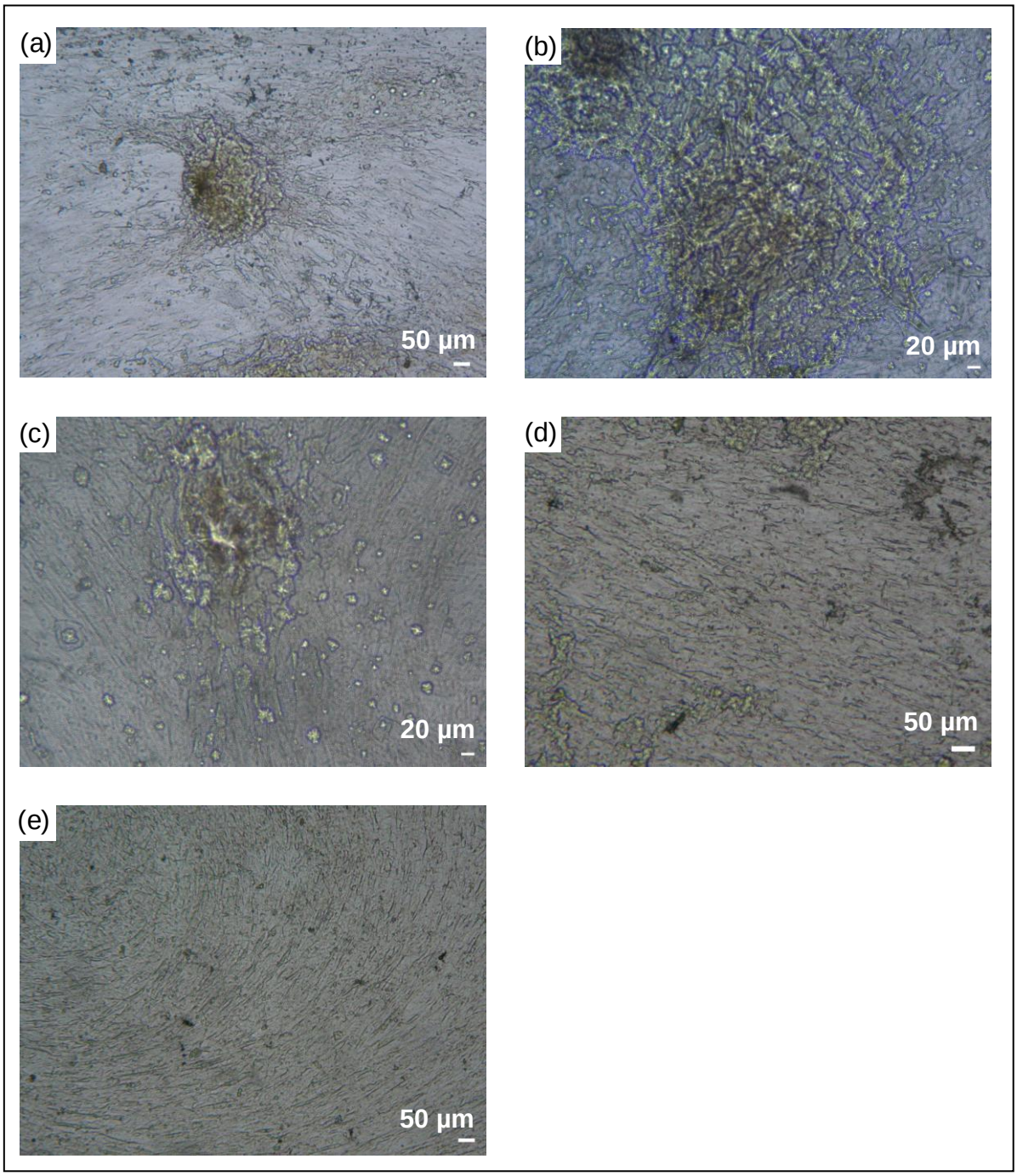

Figure 18. Mineral deposition via von Kossa staining of hMSCs on the PA-RGDS nanomatrix after days 28 (a) and 35 (b). Additional von Kossa images after 35 days for PA-DGEA (c), PA-KRSR (d), and glass (e).

Mineral deposition in the cellular environment serves as a late stage marker, signifying complete osteogenic differentiation (Satija et al., 2007). To investigate mineralization, von Kossa staining was used to qualitatively assess each of the PA nanomatrix coatings and glass (control), shown in Figure 17. Significantly more mineral deposition (brownish-black precipitates) was detected on PA-RGDS compared to the other surface conditions. Furthermore, the stained areas for PA-RGDS generally increased in size between days 28 and 35, indicating a higher degree of mineralization. Small mineralized deposits were detected on PA-DGEA after 35 days, but the stained mineralized nodules were not as pronounced and prevalent compared to PA-RGDS. No mineralized depositions were found on the PA-KRSR coating and glass culture conditions. The positive mineral stains observed on PA-RGDS are similar to past findings that used osteogenic supplements to enhance mineralization on scaffolds functionalized with the RGDS epitope (Ho et al., 2006; Ho et al., 2005). Additionally, evidence of mineral deposits was only found on surface conditions displaying integrin-mediated ligands, as opposed to proteoglycan-mediated ligands. Overall, this demonstrates the importance of signaling peptides to mineral deposition and implies that the integrin-mediated RGDS ligand has the best capacity to direct later stage osteogenic development without the present of soluble factors.

DISCUSSION

Tissue engineering is an emerging field for regenerative medicine. Focusing on bone regeneration, the ideal strategy is to emulate the essential properties of the natural bone hierarchical structure using a bottom-up approach. Thus, a bone ECM-mimicking nanomatrix has been developed, consisting of self-assembling peptide amphiphiles synthesized with specific cell adhesive ligands that serve as a nanoscale interface for hMSCs to provide biological activity. The combination of promising cell adhesive ligands with self-assembling nanomatrices creates a novel biomimetic material. This study investigated the ability of different cell adhesive ligands inscribed into the biomimetic PA nanomatrices to influence cellular behaviors due to the resulting cell-ligand interactions, which promote either integrin or non-integrin binding. The goal was to provide insight into directly controlling osteogenic differentiation based only on receptor mediated activation of the hMSCs by the cell adhesive ligand signals. Additionally, no aid from outside factors, such as media supplements or growth factors, was provided, divergent from almost all past osteogenic differentiation studies.

For all experiments, cell studies were conducted on two-dimensional PA nanomatrix coatings, created by solvent evaporation from an aqueous PA solution (0.1% wt.). After all the designed PAs were synthesized, self-assembly for each was successfully achieved, as verified by TEM imaging, due to the increased concentration and aggregation. This resulted in the formation of higher ordered structures, specifically cylindrical micelle nanofibers, which assembled together to create uniform microscale environments. Specifically, consistent PA coating surfaces made up of multiple layers of

nanofiber meshworks stacked on top of each other were found for all three PA conditions, justifying that any experimental differences observed in cellular behavior were based on the cell adhesive ligands functionalized within the PA nanomatrix coatings The influences of various cell adhesive ligands presented by the PA nanofibers were first tested with short-term cellular studies, focusing on initial attachment and proliferation. The PA-RGDS nanomatrix was found to be the best surface condition for initial hMSC attachment, demonstrating significantly more cell attachment after 1 and 4 hours than PA-DGEA and PA-KRSR at both time points. PA-DGEA also showed greater cell attachment than PA-KRSR after 1 and 4 hours of incubation. Conversely, cell proliferation analyzed by PCNA staining revealed no significant differences between the three PA nanomatrix coatings for 24 and 48 hours. Altogether, these results clearly prove that hMSCs can recognize and discern between the specific cell adhesive ligands incorporated into the PA nanomatrices during initial cell attachment, showing that these ligand signals are capable of eliciting different cellular responses. However, once the hMSCs are attached to the PA coatings, the seeded cells are able to proliferate at relatively the same rate for both 24 and 48 hours, setting an equal proliferative starting point for extended observations. Thus, these short-term experiments serve as a gateway to evaluating osteogenic differentiation over longer incubation periods.

Typically, studies researching the osteogenic differentiation of mesenchymal stem cells utilize media supplements, such as dexamethasone, β-glycerol phosphate, and ascorbic acid, as described previously in literature (Bobis et al., 2006; Gregory et al., 2005; Hu, Winn, Krajbich, & Hollinger, 2003; Kimelman et al., 2007; Yang et al., 2005). In our evaluations, osteogenic differentiation is promoted only by the ligand-mediated

bindings presented by the PA nanomatrix coatings. ALP activity and OPN secretion from the hMSCs over 21 days were used to initially assess differentiation. Based on ALP activity and OPN secretion results, the PA-RGDS nanomatrix proved to be the best candidate. ALP activity increased significantly over time on PA-RGDS and was found to be much greater on this surface compared to the other PA coatings on days 14 and 21. Additionally, OPN secretion, another osteogenic marker, again supported the differentiating potential of the PA-RGDS nanomatrix, as this coating produced a significant increase for days 19-21 relative to the preceding incubation time points.

Surprisingly, for both of these differentiation marker evaluations, the values for ALP activity and OPN secretion expressed for all PA nanomatrix conditions never fully peaked over the 21 day incubation. As seen in past literature, it had been expected that the initial differentiation markers would peak around two weeks before decreasing slightly, followed by signs of mineralization during the third week (Datta, Holtorf, Sikavitsas, Jansen, & Mikos, 2005; Jackson et al., 2007; Long, 2001; Shin et al., 2005). Since the ALP activity and OPN secretion results indicate that later stage mineralization was not reached after 21 days, possibly due to lack of supplemental factors, the cell morphology and mineral deposition evaluations were adjusted accordingly and expanded up to 35 days. Over the 35 day incubation, hMSC morphology and mineralization via von Kossa staining were both assessed qualitatively to further characterize osteogenic differentiation. Characteristic osteogenic morphology progression was observed from the hMSCs seeded on the integrin-mediated PA-RGDS nanomatrix in numerous regions throughout the sample coating surfaces. The cells changed from spindle-shape to cuboidal, first showing signs at day 14. As incubation progressed, the cuboidal

morphology became more pronounced, forming multilayered nodular clusters, thus indicating osteogenesis. PA-DGEA, another integrin-mediated nanomatrix, was the only other surface coating to display instances of this morphological change, as a few select multilayered cuboidal colonies were recorded on day 35. No evidence of osteogenic morphology was detected on the non-integrin binding nanomatrix presented by PA-KRSR. The von Kossa stains served as validation for these morphological signs of osteogenic differentiation, providing evidence of mineralization. The PA-RGDS stains showed mineralized deposits by days 28 and 35, indicating the maturation of osteogenic development. Again, PA-DGEA was the only other surface to display positive von Kossa stains, as a few mineral nodules were observed on day 35. Overall, based on the results for ALP activity, OPN secretion, cell morphology, and mineralization via von Kossa staining, the PA-RGDS nanomatrix emerged as the best candidate for directing osteogenic differentiation based solely on ECM-mimicking cell adhesive ligands and without supplemental aid.

Interestingly, integrin-mediated cell binding exerted the greatest influence on controlling cellular behaviors, specifically the RGDS ligand. Though, the integrin-specific DGEA epitope also proved more effective than the proteoglycan-mediated KRSR ligand. The increased hMSC attachment on PA-RGDS was expected, as this behavior has been reviewed extensively (Hersel et al., 2003). The observed osteogenic differentiation results were also greatly affected by the RGDS ligand-cell interactions. This finding expands upon previous studies that found the RGDS ligand to promote osteogenic development when synergistically combined with supplements (Behravesh & Mikos, 2003; Hu et al., 2003; Yang et al., 2005) or without (Shin et al., 2005).

Additionally, the differentiation results for the PA-RGDS nanomatrix could possibly be correlated to the increased initial hMSC attachment that was observed on this surface coating, as Harbers and Healy reported that an initial cell attachment threshold is needed to support significant mineralization (Harbers & Healy, 2005). Regarding the other PA coatings, the PA-DGEA nanomatrix did display some signs of differentiation. However, it may have a greater impact on mature osteoblast cells, as this ligand signal has been shown to promote integrin-mediated mineralization with fully differentiated osteogenic cells (Xiao, Wang, Benson, Karsenty, & Franceschi, 1998). The proteoglycan-mediated binding presented by the PA-KRSR nanomatrix yielded no evidence of controlling osteogenic differentiation. It appears that the KRSR ligand is only beneficial when utilized in conjunction with other bioadhesive sequences (Dee, Andersen, & Bizios, 1998). Taken together, this demonstrates that the RGDS ligand, in the absence of stimulatory factors, leads to the activation of the hMSC signaling pathways responsible for directing osteogenic differentiation by integrin-mediated binding.

As a bone regeneration strategy, this research presents a biomimetic approach to tissue engineering by mimicking the native bone tissue environment at the nanoscale level and incorporating bioactive peptide signals isolated from ECM molecules. However, many challenges remain to fully develop this system to the necessary clinical level. Numerous factors will need to be considered and explored, such as adapting the osteogenic differentiation time to the biologically correct bone healing rate, optimizing the density of the ligand signals presented by controlling the concentration of the PA solution, and eventually transitioning from a 2-D to a 3-D system. To our advantage, PAs are a very adaptable biomaterial that allows for the necessary fine-tuning required to

meet these biomedical challenges and for the continued development of this biomimetic regenerative approach.

This research model has potential for broad applications outside of bone regeneration, as it provides fundamental insight into not only understanding essential natural bone tissue formation, but also a new versatile strategy to regenerate a variety of tissues by closely mimicking the principle of natural tissue formation. Furthermore, as a self-assembling biomimetic nanomatrix, the PAs have the capacity to be coated onto other biomedical devices, such as bone fixation implants or cardiovascular stents, functionalizing them with selective bioactivity. Presently, the future plans include designing quantitative real time-PCR gene analysis experiments to detect osteogenic differentiation markers, performing positive and negative control experiments with and without osteogenic media supplements to evaluate possible synergistic effects, investigating composite PA nanomatrices that combine two or more adhesive ligands, incorporating the HA/TTCP inorganic component, and cell encapsulation studies with 3-D self-assembling PA gels. The results from all conducted 2-D studies clearly show that this biomimetic approach allows for osteoprogenitor cells, such as hMSCs, to be directed to undergo osteogenic differentiation in a nanomatrix inscribed with isolated ECM isolated signals.

CONCLUSIONS

Natural tissue formation is a well-organized process that starts at the nanoscale level. Therefore, to best facilitate tissue regenerative needs, a biomimetic approach is needed to capture the complex hierarchical order of native tissue. Focusing on bone tissue regeneration, we have investigated self-assembling PA nanofibers that present ECM-mimicking cell adhesive ligands, tailored for specific bioactivity and functionalized with enzyme degradable sites to allow for natural tissue remodeling. This biomimetic construct served as an interface for hMSCs, introduced to provide biological activity. The abilities of the different cell-ligand interactions presented by the PA nanomatrices to influence osteogenic differentiation and other cellular behaviors without the presence of soluble factors were explored. From our studies, the integrin-mediated PA-RGDS nanomatrix was found to have the most promise, demonstrating the importance of integrin-specific binding for osteogenic differentiation. Overall, the incorporation of ECM-mimicking signals, particularly the RGDS ligand, into self-assembling PA nanomatrices is an ideal biomimetic strategy and has great potential for bone tissue regeneration.

APPENDIX

THE UNIVERSITY OF ALABAMA AT BIRMINGHAM

Institutional Review Board for Human Use

DATE: 3/21/08

MEMORANDUM

TO: **Ho-Wook Jun**
Principal Investigator

FROM: Sheila Moore, CIP
Director, IRB

RE: Request for Determination—Human Subjects Research
IRB Protocol #N080319010 – ECM mimic organic/inorganic composite nano matrix for bone tissue regeneration

An IRB Member has reviewed your application for Designation of Not Human Subjects Research for above reference proposal.

The reviewer has determined that this proposal is **not** subject to FDA regulations and is **not** Human Subjects Research. Note that any changes to the project should be resubmitted to the Office of the IRB for determination.

SM/lg

470 Administration Building
701 20th Street South
205.934.3789
Fax 205.934.1301
irb@uab.edu

The University of
Alabama at Birmingham
Mailing Address:
AB 470
1530 3RD AVE S
BIRMINGHAM AL 35294-0104

LIST OF REFERENCES

Accardo, A., Tesauro, D., Mangiapia, G., Pedone, C., & Morelli, G. (2007). Nanostructures by self-assembling peptide amphiphile as potential selective drug carriers. *Peptide Science, 88*(2), 115-121.

America's Bone Health: The State of Osteoporosis and Low Bone Mass in our Nation. (2002). Retrieved from National Osteoporosis Foundation.

Arrington, E. D., Smith, W. J., Chambers, H. G., Bucknell, A. L., & Davino, N. A. (1996). Complications of iliac crest bone graft harvesting. *Clin Orthop Relat Res*(329), 300-309.

Athanasiou, K. A., Niederauer, G. G., & Agrawal, C. M. (1996). Sterilization, toxicity, biocompatibility and clinical applications of polylactic acid/polyglycolic acid copolymers. *Biomaterials, 17*(2), 93-102.

Balasundaram, G., & Webster, T. J. (2007). Increased osteoblast adhesion on nanograined Ti modified with KRSR. *J Biomed Mater Res A, 80*(3), 602-611.

Behravesh, E., & Mikos, A. G. (2003). Three-dimensional culture of differentiating marrow stromal osteoblasts in biomimetic poly(propylene fumarate-co-ethylene glycol)-based macroporous hydrogels. *J Biomed Mater Res A, 66*(3), 698-706.

Beniash, E., Hartgerink, J. D., Storrie, H., Stendahl, J. C., & Stupp, S. I. (2005). Self-assembling peptide amphiphile nanofiber matrices for cell entrapment. *Acta Biomater, 1*(4), 387-397.

Bobis, S., Jarocha, D., & Majka, M. (2006). Mesenchymal stem cells: characteristics and clinical applications. *Folia Histochem Cytobiol, 44*(4), 215-230.

Bridwell, K. H., O'Brien, M. F., Lenke, L. G., Baldus, C., & Blanke, K. (1994). Posterior Spinal Fusion Supplemented with only Allograft Bone in Paralytic Scoliosis. Does it Work? *Spine, 19*(23), 2658-2666.

Burge, R., Dawson-Hughes, B., Solomon, D. H., Wong, J. B., King, A., & Tosteson, A. (2007). Incidence and Economic Burden of Osteoporosis-Related Fractures in the United States, 2005 2025. *Journal of Bone and Mineral Research, 22*(3), 465-475.

Carter, G. (1999). Harvesting and implanting allograft bone. *Aorn J, 70*(4), 660-670; quiz 672-666.

Celis, J. E., & Celis, A. (1985). Cell cycle-dependent variations in the distribution of the nuclear protein cyclin proliferating cell nuclear antigen in cultured cells: subdivision of S phase. *Proc Natl Acad Sci U S A, 82*(10), 3262-3266.

Chen, F. H., Rousche, K. T., & Tuan, R. S. (2006). Technology Insight: Adult Stem Cells in Cartilage Regeneration and Tissue Engineering. *Nature Clinical Practice: Rheumatology, 2*(7), 373-382.

Cornell, C. N. (1999). Osteoconductive materials and their role as substitutes for autogenous bone grafts. *Orthop Clin North Am, 30*(4), 591-598.

Cowan, C. M., Soo, C., Ting, K., & Wu, B. (2005). Evolving concepts in bone tissue engineering. *Curr Top Dev Biol, 66*, 239-285.

Daley, W. P., Peters, S. B., & Larsen, M. (2008). Extracellular matrix dynamics in development and regenerative medicine. *J Cell Sci, 121*(Pt 3), 255-264.

Datta, N., Holtorf, H. L., Sikavitsas, V. I., Jansen, J. A., & Mikos, A. G. (2005). Effect of bone extracellular matrix synthesized in vitro on the osteoblastic differentiation of marrow stromal cells. *Biomaterials, 26*(9), 971-977.

Dee, K. C., Andersen, T. T., & Bizios, R. (1998). Design and function of novel osteoblast-adhesive peptides for chemical modification of biomaterials. *J Biomed Mater Res, 40*(3), 371-377.

Fibbe, W. E., & Noort, W. A. (2003). Mesenchymal Stem Cells and Hematopoietic Stem Cell Transplantation. *Ann NY Acad Sci, 996*(1), 235-244.

Friedenstein, A. J., Gorskaja, J. F., & Kulagina, N. N. (1976). Fibroblast precursors in normal and irradiated mouse hematopoietic organs. *Exp Hematol, 4*(5), 267-274.

Garcia, R. L., Coltrera, M. D., & Gown, A. M. (1989). Analysis of proliferative grade using anti-PCNA/cyclin monoclonal antibodies in fixed, embedded tissues. Comparison with flow cytometric analysis. *Am J Pathol, 134*(4), 733-739.

Gau, Y. L., Lonstein, J. E., Winter, R. B., Koop, S., & Denis, F. (1991). Luque-Galveston procedure for correction and stabilization of neuromuscular scoliosis and pelvic obliquity: a review of 68 patients. *J Spinal Disord, 4*(4), 399-410.

Giannoudis, P. V., Dinopoulos, H., & Tsiridis, E. (2005). Bone substitutes: an update. *Injury, 36 Suppl 3*, S20-27.

Gregory, C. A., Prockop, D. J., & Spees, J. L. (2005). Non-hematopoietic bone marrow stem cells: molecular control of expansion and differentiation. *Exp Cell Res, 306*(2), 330-335.

Guler, M. O., Hsu, L., Soukasene, S., Harrington, D. A., Hulvat, J. F., & Stupp, S. I. (2006). Presentation of RGDS epitopes on self-assembled nanofibers of branched peptide amphiphiles. *Biomacromolecules, 7*(6), 1855-1863.

Guo, D., Xu, K., & Han, Y. (2008). The in situ synthesis of biphasic calcium phosphate scaffolds with controllable compositions, structures, and adjustable properties. *Journal of Biomedical Materials Research Part A, 9999*(9999), NA.

Gupta, H. S., Wagermaier, W., Zickler, G. A., Raz-Ben Aroush, D., Funari, S. S., Roschger, P., et al. (2005). Nanoscale deformation mechanisms in bone. *Nano Lett, 5*(10), 2108-2111.

Harbers, G. M., & Healy, K. E. (2005). The effect of ligand type and density on osteoblast adhesion, proliferation, and matrix mineralization. *J Biomed Mater Res A, 75*(4), 855-869.

Harrington, D. A., Cheng, E. Y., Guler, M. O., Lee, L. K., Donovan, J. L., Claussen, R. C., et al. (2006). Branched peptide-amphiphiles as self-assembling coatings for tissue engineering scaffolds. *J Biomed Mater Res A, 78*(1), 157-167.

Hartgerink, J. D. (2004). Covalent capture: a natural complement to self-assembly. *Current Opinion in Chemical Biology, 8*(6), 604-609.

Hartgerink, J. D., Beniash, E., & Stupp, S. I. (2001). Self-assembly and mineralization of peptide-amphiphile nanofibers. *Science, 294*(5547), 1684-1688.

Hartgerink, J. D., Beniash, E., & Stupp, S. I. (2002). Peptide-amphiphile nanofibers: a versatile scaffold for the preparation of self-assembling materials. *Proc Natl Acad Sci U S A, 99*(8), 5133-5138.

Hasenbein, M. E., Andersen, T. T., & Bizios, R. (2002). Micropatterned surfaces modified with select peptides promote exclusive interactions with osteoblasts. *Biomaterials, 23*(19), 3937-3942.

Hayashi, O., Katsube, Y., Hirose, M., Ohgushi, H., & Ito, H. (2008). Comparison of osteogenic ability of rat mesenchymal stem cells from bone marrow, periosteum, and adipose tissue. *Calcif Tissue Int, 82*(3), 238-247.

Hersel, U., Dahmen, C., & Kessler, H. (2003). RGD modified polymers: biomaterials for stimulated cell adhesion and beyond. *Biomaterials, 24*(24), 4385-4415.

Ho, M. H., Hou, L. T., Tu, C. Y., Hsieh, H. J., Lai, J. Y., Chen, W. J., et al. (2006). Promotion of cell affinity of porous PLLA scaffolds by immobilization of RGD peptides via plasma treatment. *Macromol Biosci, 6*(1), 90-98.

Ho, M. H., Wang, D. M., Hsieh, H. J., Liu, H. C., Hsien, T. Y., Lai, J. Y., et al. (2005). Preparation and characterization of RGD-immobilized chitosan scaffolds. *Biomaterials, 26*(16), 3197-3206.

Hosseinkhani, H., Hosseinkhani, M., Khademhosseini, A., & Kobayashi, H. (2007). Bone regeneration through controlled release of bone morphogenetic protein-2 from 3-D tissue engineered nano-scaffold. *Journal of Controlled Release, 117*(3), 380-386.

Hosseinkhani, H., Hosseinkhani, M., Khademhosseini, A., Kobayashi, H., & Tabata, Y. (2006). Enhanced angiogenesis through controlled release of basic fibroblast growth factor from peptide amphiphile for tissue regeneration. *Biomaterials, 27*(34), 5836-5844.

Hosseinkhani, H., Hosseinkhani, M., Tian, F., Kobayashi, H., & Tabata, Y. (2006). Osteogenic differentiation of mesenchymal stem cells in self-assembled peptide-amphiphile nanofibers. *Biomaterials, 27*(22), 4079-4086.

Hosseinkhani, H., Hosseinkhani, M., Tian, F., Kobayashi, H., & Tabata, Y. (2007). Bone Regeneration on a Collagen Sponge Self-Assembled Peptide-Amphiphile Nanofiber Hybrid Scaffold. *Tissue Engineering, 13*(1), 11-19.

Hu, Y., Winn, S. R., Krajbich, I., & Hollinger, J. O. (2003). Porous polymer scaffolds surface-modified with arginine-glycine-aspartic acid enhance bone cell attachment and differentiation in vitro. *J Biomed Mater Res A, 64*(3), 583-590.

Israelachvili, J. N., Mitchell, D. J., & Ninham, B. W. (1977). Theory of Self-Assembly of Lipid Bilayers and Vesicles. *Biochimica et Biophysica Acta, 470*(2), 185-201.

Jackson, L., Jones, D. R., Scotting, P., & Sottile, V. (2007). Adult mesenchymal stem cells: differentiation potential and therapeutic applications. *J Postgrad Med, 53*(2), 121-127.

Jun, H. W., Yuwono, V., Paramonov, S. E., & Hartgerink, J. D. (2005). Enzyme-Mediated Degradation of Peptide-Amphiphile Nanofiber Networks. *Advanced Materials, 17*(21), 2612-2617.

Kim, H., Camata, R., Vohra, Y., & Lacefield, W. (2005). Control of phase composition in hydroxyapatite/tetracalcium phosphate biphasic thin coatings for biomedical applications. *Journal of Materials Science: Materials in Medicine, 16*(10), 961-966.

Kimelman, N., Pelled, G., Helm, G. A., Huard, J., Schwarz, E. M., & Gazit, D. (2007). Review: gene- and stem cell-based therapeutics for bone regeneration and repair. *Tissue Eng, 13*(6), 1135-1150.

Kleinman, H. K., Philp, D., & Hoffman, M. P. (2003). Role of the extracellular matrix in morphogenesis. *Curr Opin Biotechnol, 14*(5), 526-532.

Kulterer, B., Friedl, G., Jandrositz, A., Sanchez-Cabo, F., Prokesch, A., Paar, C., et al. (2007). Gene expression profiling of human mesenchymal stem cells derived from bone marrow during expansion and osteoblast differentiation. *BMC Genomics, 8*, 70.

LeBaron, R. G., & Athanasiou, K. A. (2000). Extracellular matrix cell adhesion peptides: functional applications in orthopedic materials. *Tissue Eng, 6*(2), 85-103.

Long, M. W. (2001). Osteogenesis and bone-marrow-derived cells. *Blood Cells Mol Dis, 27*(3), 677-690.

Lowik, D. W. P. M., & Hest, J. C. M. v. (2004). Peptide based amphiphiles. *Chemical Society Reviews, 33*(4), 234-245.

Lynch, D. A., Clarke, A. M., Jackson, P., Axon, A. T., Dixon, M. F., Quirke, P (1994). Comparison of labelling by bromodeoxyuridine, MIB-1, and proliferating cell nuclear antigen in gastric mucosal biopsy specimens. *J Clin Pathol, 47*(2), 122-125.

Mardilovich, A., Craig, J. A., McCammon, M. Q., Garg, A., & Kokkoli, E. (2006). Design of a novel fibronectin-mimetic peptide-amphiphile for functionalized biomaterials. *Langmuir, 22*(7), 3259-3264.

Mauney, J. R., Kirker-Head, C., Abrahamson, L., Gronowicz, G., Volloch, V., & Kaplan, D. L. (2006). Matrix-mediated retention of in vitro osteogenic differentiation potential and in vivo bone-forming capacity by human adult bone marrow-derived mesenchymal stem cells during ex vivo expansion. *J Biomed Mater Res A, 79*(3), 464-475.

McAndrew, M. P., Gorman, P. W., & Lange, T. A. (1988). Tricalcium phosphate as a bone graft substitute in trauma: preliminary report. *J Orthop Trauma, 2*(4), 333-339.

McCarthy, R. E., Peek, R. D., Morrissy, R. T., & Hough Jr, A. J. (1986). Allograft Bone in Spinal Fusion for Paralytic Scoliosis. *Journal of Bone Joint Surge American, 68*(3), 370-375.

Mizuno, M., Fujisawa, R., & Kuboki, Y. (2000). Type I collagen-induced osteoblastic differentiation of bone-marrow cells mediated by collagen-alpha2beta1 integrin interaction. *J Cell Physiol, 184*(2), 207-213.

Mizuno, M., & Kuboki, Y. (2001). Osteoblast-Related Gene Expression of Bone Marrow Cells during the Osteoblastic Differentiation Induced by Type I Collagen. *J Biochem, 129*(1), 133-138.

Na, K., Kim, S. W., Sun, B. K., Woo, D. G., Yang, H. N., Chung, H. M., et al. (2007). Osteogenic differentiation of rabbit mesenchymal stem cells in thermo-reversible hydrogel constructs containing hydroxyapatite and bone morphogenic protein-2 (BMP-2). *Biomaterials, 28*(16), 2631-2637.

Nagase, H., & Fields, G. B. (1996). Human matrix metalloproteinase specificity studies using collagen sequence-based synthetic peptides. *Peptide Science, 40*(4), 399-416.

Nelson, F. R. T., Brighton, C. T., Ryaby, J., Simon, B. J., Nielson, J. H., Lorich, D. G., et al. (2003). Use of Physical Forces in Bone Healing. *J Am Acad Orthop Surg, 11*(5), 344-354.

Osteoporosis Prevention, Diagnosis, and Therapy Conference: Consensus Statement. (2000). Retrieved from National Institute of Health.

Paramonov, S. E., Jun, H. W., & Hartgerink, J. D. (2006). Self-Assembly of Peptide-Amphiphile Nanofibers: The Roles of Hydrogen Bonding and Amphiphilic Packing. *J. Am. Chem. Soc., 128*(22), 7291-7298.

Pierschbacher, M. D., & Ruoslahti, E. (1984). Cell attachment activity of fibronectin can be duplicated by small synthetic fragments of the molecule. *Nature, 309*(5963), 30-33.

Rajangam, K., Behanna, H. A., Hui, M. J., Han, X., Hulvat, J. F., Lomasney, J. W., et al. (2006). Heparin Binding Nanostructures to Promote Growth of Blood Vessels. *Nano Lett., 6*(9), 2086-2090.

Ratner, B. D. H., A.S.; Schoen F.; Lemons, J.E. (1996). *Biomaterials Science: An Introduction to Materials in Medicine*. San Diego, CA: Academic Press.

Rezler, E. M., Khan, D. R., Lauer-Fields, J., Cudic, M., Baronas-Lowell, D., & Fields, G. B. (2007). Targeted Drug Delivery Utilizing Protein-Like Molecular Architecture. *J. Am. Chem. Soc., 129*(16), 4961-4972.

Rho, J.-Y., Kuhn-Spearing, L., & Zioupos, P. (1998). Mechanical properties and the hierarchical structure of bone. *Medical Engineering & Physics, 20*(2), 92-102.

Sargeant, T. D., Guler, M. O., Oppenheimer, S. M., Mata, A., Satcher, R. L., Dunand, D. C., et al. (2008). Hybrid bone implants: self-assembly of peptide amphiphile nanofibers within porous titanium. *Biomaterials, 29*(2), 161-171.

Sargeant, T. D., Rao, M. S., Koh, C.-Y., & Stupp, S. I. (2008). Covalent functionalization of NiTi surfaces with bioactive peptide amphiphile nanofibers. *Biomaterials, 29*(8), 1085-1098.

Satija, N. K., Gurudutta, G. U., Sharma, S., Afrin, F., Gupta, P., Verma, Y. K., et al. (2007). Mesenchymal stem cells: molecular targets for tissue engineering. *Stem Cells Dev, 16*(1), 7-23.

Schlegel, K. A., Donath, K., Rupprecht, S., Falk, S., Zimmermann, R., Felszeghy, E., et al. (2004). De novo bone formation using bovine collagen and platelet-rich plasma. *Biomaterials, 25*(23), 5387-5393.

Shin, H., Jo, S., & Mikos, A. G. (2003). Biomimetic materials for tissue engineering. *Biomaterials, 24*(24), 4353-4364.

Shin, H., Temenoff, J. S., Bowden, G. C., Zygourakis, K., Farach-Carson, M. C., Yaszemski, M. J., et al. (2005). Osteogenic differentiation of rat bone marrow stromal cells cultured on Arg-Gly-Asp modified hydrogels without dexamethasone and beta-glycerol phosphate. *Biomaterials, 26*(17), 3645-3654.

Silva, G. A., Czeisler, C., Niece, K. L., Beniash, E., Harrington, D. A., Kessler, J. A., et al. (2004). Selective differentiation of neural progenitor cells by high-epitope density nanofibers. *Science, 303*(5662), 1352-1355.

Singh, D., de la Cinta Lorenzo-Martin, M., Gutiérrez-Mora, F., Routbort, J. L., & Case, E. D. (2006). Self-joining of zirconia/hydroxyapatite composites using plastic deformation process. *Acta Biomaterialia, 2*(6), 669-675.

Statistical Abstract for the United States: Section 3 Health and Nutrition. (2008). Retrieved from U.S. Census Bureau <http://www.census.gov/statab/www/>.

Stefanidakis, M., & Koivunen, E. (2006). Cell-surface association between matrix metalloproteinases and integrins: role of the complexes in leukocyte migration and cancer progression. *Blood, 108*(5), 1441-1450.

Stendahl, J. C., Rao, M. S., Guler, M. O., & Stupp, S. I. (2006). Intermolecular Forces in the Self-Assembly of Peptide Amphiphile Nanofibers. *Advanced Functional Materials, 16*(4), 499-508.

Stevens, M. M., & George, J. H. (2005). Exploring and Engineering the Cell Surface Interface. *Science, 310*(5751), 1135-1138.

Storrie, H., Guler, M. O., Abu-Amara, S. N., Volberg, T., Rao, M., Geiger, B., et al. (2007). Supramolecular crafting of cell adhesion. *Biomaterials, 28*(31), 4608-4618.

Streuli, C. (1999). Extracellular matrix remodelling and cellular differentiation. *Current Opinion in Cell Biology, 11*(5), 634-640.

Wiltfang, J., Kloss, F. R., Kessler, P., Nkenke, E., Schultze-Mosgau, S., Zimmermann, R., et al. (2004). Effects of platelet-rich plasma on bone healing in combination with autogenous bone and bone substitutes in critical-size defects. An animal experiment. *Clin Oral Implants Res, 15*(2), 187-193.

Woll, N. L., Heaney, J. D., & Bronson, S. K. (2006). Osteogenic nodule formation from single embryonic stem cell-derived progenitors. *Stem Cells Dev, 15*(6), 865-879.

Xiao, G., Wang, D., Benson, M. D., Karsenty, G., & Franceschi, R. T. (1998). Role of the alpha2-integrin in osteoblast-specific gene expression and activation of the Osf2 transcription factor. *J Biol Chem, 273*(49), 32988-32994.

Yang, F., Williams, C. G., Wang, D. A., Lee, H., Manson, P. N., & Elisseeff, J. (2005). The effect of incorporating RGD adhesive peptide in polyethylene glycol diacrylate hydrogel on osteogenesis of bone marrow stromal cells. *Biomaterials, 26*(30), 5991-5998.

Zhang, A. X., Yu, W. H., Ma, B. F., Yu, X. B., Mao, F. F., Liu, W., et al. (2007). Proteomic identification of differently expressed proteins responsible for osteoblast differentiation from human mesenchymal stem cells. *Mol Cell Biochem, 304*(1-2), 167-179.